Research Square

Preprints are preliminary reports that have not undergone peer review.
They should not be considered conclusive, used to inform clinical practice,
or referenced by the media as validated information.

Seismic Behaviour of UHM-CFRP-Strengthened RC Frame Buildings

Thokchom Amarishwar Singh

amarishwarthokchom@gmail.com

National Institute of Technology Manipur

Mayengbam Sunil Singh

National Institute of Technology Manipur

Research Article

Keywords: Ultra-High Modulus Carbon Fiber–Reinforced Polymers, Direct Displacement Based Design, Inter-storey drift ratio, Building stiffness ratio, Reinforced concrete

Posted Date: November 4th, 2026

DOI: https://doi.org/10.21203/rs.3.rs-11344334/v1

License: This work is licensed under a Creative Commons Attribution 4.0 International License.
Read Full License

Additional Declarations: No competing interests reported.

Seismic Behaviour of UHM-CFRP-Strengthened RC Frame Buildings

First Author: Thokchom Amarishwar Singh*

Research Scholar

Department of Civil Engineering, National Institute of Technology Manipur, Imphal, India;

Second Author: Mayengbam Sunil Singh

Associate professor

Department of Civil Engineering, National Institute of Technology Manipur, Langol, Imphal, India

*Corresponding author e-mail: amarishwarthokchom@gmail.com

First Author: amarishwarthokchom@gmail.com

Second Author: mayengbamsunil5@gmail.com

Seismic Behaviour of UHM-CFRP-Strengthened RC Frame Buildings

Thokchom Amarishwar Singh[1*] & Mayengbam Sunil Singh[1]

National Institute of Technology Manipur, Langol, Imphal – 795004, India

*Corresponding author e-mail: amarishwarthokchom@gmail.com

First Author: amarishwarthokchom@gmail.com

Second Author: mayengbamsunil5@gmail.com

Abstract:

Carbon fibre-reinforced polymer (CFRP) composites have emerged as an effective solution for enhancing the seismic performance of reinforced concrete (RC) structures. While previous studies have predominantly focused on the behaviour of CFRP-strengthened structural members, limited attention has been given to their influence on the global seismic response of RC frame buildings. This study evaluates the effectiveness of CFRP strengthening in improving the seismic performance of RC frame buildings with reduced concrete strength. 4-, 6-, 8-, and 10-storey RC frame buildings are designed using the Direct Displacement-Based Design (DDBD) methodology with a target inter-storey drift ratio (IDR) of 2%, based on the Eurocode 8 design response spectrum corresponding to a peak ground acceleration (PGA) of 0.45 g and a damping ratio of 5%. Numerical models of CFRP-strengthened beams and columns are validated against published experimental results. Buildings designed with M25 concrete are considered as the reference models, and the concrete grade is subsequently reduced to M20, M15 and M10 to simulate strength deterioration. Nonlinear time-history analyses are carried out using spectrum-compatible ground motions. Based on the analytical results, empirical equations are developed to predict the IDR ratio and building stiffness ratio as functions of concrete grade and are validated using independent building models with different plan configurations and heights. The results indicate that CFRP strengthening considerably reduces inter-storey drift and increases the lateral stiffness of RC frame buildings, particularly for buildings with lower concrete strength. The proposed equations provide a practical and reliable tool for estimating the seismic response of CFRP-strengthened RC buildings.

Keywords: Ultra-High Modulus Carbon Fiber–Reinforced Polymers, Direct Displacement Based Design, Inter-storey drift ratio, Building stiffness ratio, Reinforced concrete.

1. Introduction

The seismic vulnerability of existing reinforced concrete (RC) buildings has necessitated the development of strengthening techniques capable of enhancing structural strength, stiffness, ductility, and deformation capacity. Conventional interventions such as concrete and steel jacketing and addition of shear walls can effectively improve member capacity and confinement, but may increase structural weight and stiffness, enlarge member dimensions, and involve considerable construction and labour requirements (Thermou and Elnashai, 2006; Engindeniz et al., 2005). These limitations have motivated the adoption of externally bonded fibre-reinforced polymer (FRP) composites, which offer high strength-to-weight ratio, high tensile strength and stiffness, corrosion resistance, and relatively limited geometric intrusion into existing members (Thermou and Bousselham, 2010; Bakis et al., 2002). However, the effectiveness of FRP strengthening remains dependent on composite–concrete bond behaviour, substrate condition, strengthening configuration, and durability; premature debonding and fire vulnerability are among the important limitations of externally bonded systems (Ji et al., 2013).

FRP strengthening has been extensively investigated at the RC member level. For columns, externally bonded FRP jackets provide confinement to the concrete core and can enhance strength, ductility, and deformation capacity. The confinement efficiency is influenced by parameters such as section geometry, corner radius, and number of FRP layers, while stress–strain models have been developed to quantify the resulting confined-concrete response (Teng et al., 2002; Lam et al., 2003; Sheikh et al., 2007; Eid et al., 2017). Experimental investigations have further demonstrated that FRP jacketing can restrain lap-splice slip, enhance flexural ductility, and modify brittle shear-controlled failure towards a more desirable flexural response (Bousias et al., 2007; Del et al., 2017; Seible et al., 1997). Similar improvements in strength and deformation capacity have been reported for deficient and short RC columns strengthened with FRP/CFRP systems (Binici et al., 2007; Ozcan et al., 2008; Colomb et al., 2008; Promis et al., 2009; Ghobarah et al., 2000). More recently, Zhu et al., (2025) demonstrated that FRP-retrofitted rectangular RC columns can maintain stable structural response under oblique and bidirectional seismic loading, highlighting the effectiveness of FRP confinement under multidirectional seismic demands.

At the beam level, externally bonded FRP laminates have been shown to enhance flexural and shear resistance, with the response depending strongly on the strengthening and anchorage configuration (Mosallam et al., 2007). Nevertheless, interfacial debonding can limit the mobilisation of the tensile capacity of the composite, as interfacial shear and peeling stresses may govern failure near the termination of bonded FRP plates. Increasing CFRP thickness or

bond length beyond an optimum range does not necessarily produce proportional capacity enhancement and may promote premature debonding (Rabinovitch et al., 2003; Li et al., 2006). These findings establish that the effectiveness of externally bonded FRP systems is governed by the coupled behaviour of the composite, adhesive interface, concrete substrate, and strengthening configuration.

Among the different FRP systems, carbon-fibre-reinforced polymer (CFRP) has received particular attention for seismic rehabilitation because of its high tensile strength and stiffness with minimal additional structural weight. CFRP strengthening has been demonstrated to improve the flexural response of RC beams and the lateral response of RC columns, while appropriate confinement and strengthening configuration are essential for achieving favourable failure mechanisms (Esfahania et al., 2006; Alaa et al., 2022). CFRP/FRP strengthening has also been applied to beam-column joints, where it can enhance joint shear resistance, stiffness, and energy dissipation and upgrade deficient connections **(**Antonopoulos et al., 2003; Prota et al., 2004; Karayannis et al., 2008**).**

Research subsequently progressed from individual members and joints towards global RC-frame response. Full-scale and numerical investigations have demonstrated that FRP/CFRP retrofit can improve displacement capacity, drift resistance, lateral strength, ductility, and the distribution of plastic deformation in multi-storey RC frames (Balsamo et al., 2005; Ludovico et al., 2008; Pampanin et al., 2007; Niroomandi et al., 2010; Eslami et al., 2013**).** Performance-based optimisation studies have further shown that the amount and spatial distribution of FRP can be selected to satisfy global deformation constraints while avoiding inefficient strengthening (Zou et al., 2007; Hadigheh et al., 2014). More recent investigations have extended this framework to seismic fragility, retrofit optimisation, economic assessment, and post-earthquake field performance, demonstrating the practical applicability of FRP/CFRP retrofit to deficient RC buildings **(**Mazza et al., 2019; Jafari et al., 2023; Pohoryles et al., 2024; Vecchio et al., 2021; Işık et al., 2026**).**

Despite this extensive evidence, the majority of existing studies have focused on conventional FRP/CFRP systems, with comparatively limited investigation of the global seismic implications of ultra-high-modulus CFRP (UHM-CFRP) in multi-storey RC buildings. UHM-CFRP belongs to the CFRP family but is characterised by an exceptionally high longitudinal elastic modulus, providing the potential to influence not only strength and deformation capacity but also the stiffness characteristics of the strengthened structural system. High-modulus CFRP has demonstrated structural potential in strengthened slender structural members, while investigations of UHM-CFRP bond and fatigue behaviour have highlighted

the importance of effective interfacial stress transfer and bond integrity (Shaat and Fam, 2007; Wu et al., 2013)**.**

Despite the extensive body of research on FRP and CFRP strengthening, the available literature has predominantly addressed conventional FRP/CFRP systems at the member, connection, and complete-frame levels, whereas the global seismic implications of UHM-CFRP strengthening in multi-storey RC frame buildings remain insufficiently quantified. More specifically, the influence of the exceptionally high stiffness of UHM-CFRP on theglobal seismic response of RC buildings with degraded concrete strength has received limited attention. This issue is particularly relevant to existing RC buildings, where ageing, deterioration, or other adverse conditions may reduce the effective concrete strength and consequently alter the stiffness, strength, deformation capacity, and seismic demand of the structural system.

Accordingly, a building-level assessment is required to determine whether the enhanced stiffness and strength contribution of UHM-CFRP can effectively compensate for reductions in concrete strength and restore the seismic response of deteriorated RC buildings. Such an assessment should consider not only member-level capacity enhancement but also the resulting system-level changes in inter-storey drift, lateral stiffness, and deformation demand, while accounting for the influence of building height.

Against this background, the present study investigates the seismic response of UHM-CFRP-strengthened multi-storey RC frame buildings with different concrete grades. Four-, six-, eight-, and ten-storey buildings are considered, with M25 as the reference concrete grade and M20, M15, and M10 representing progressively reduced concrete strength. The study aims to evaluate the effectiveness of UHM-CFRP strengthening in mitigating the increase in seismic deformation demand associated with reduced concrete strength, investigate the influence of building height on inter-storey drift and lateral stiffness, and quantify the resulting improvement in global seismic performance. Furthermore, empirical relationships are developed to predict the inter-storey drift ratio and stiffness ratio as functions of concrete grade and building height, and their applicability is assessed using independent RC building configurations.

2. Validation of CFRP model

The structural models of CFRP-strengthened beams and columns adopted in this study are first validated against the experimental results reported by Esfahania et al. (2006) and Alaa et al. (2022**)** respectively. The corresponding specimen details are summarised in Table 1. In the experimental study conducted by Esfahania et al. (2006), three RC beam specimens, namely B1, B2, and B3 (Figure 1a), with identical geometric dimensions were tested under four-point

bending. Beam B1 served as the unstrengthened control specimen, providing a baseline for comparison. Beams B2 and B3 were retrofitted with single-layer and double-layer CFRP sheets respectively, externally bonded to their soffits (tension face).

Table 1: Material Properties

	Beam			Column	
Rebar					
Diameter (millimeter)	8	10	20	8	12
Yielding stress (MegaPascal)	350	365	350	530	570
Ultimate stress (MegaPascal)	459	572	570	670	710
Concrete					
Compressive strength (MegaPascal)	24.1			32.2	
FRP					
Modulus of Elasticity (GigaPascal)	240			230	
Tensile strength (GigaPascal)	3800			3530	
Ultimate strain	0.0155			0.015	
Layer thickness (millimeter)	0.176			0.125	

In the experimental study conducted by Esfahania et al. (2006), three RC column specimens, namely C1, C2, and C3 (Figure 1b), with identical geometric dimensions were subjected to axial and lateral loads applied at the top and mid-height respectively. Column C1 served as the unstrengthened control specimen, providing a baseline for comparison. Column C2 was retrofitted with a single layer of externally bonded CFRP sheet in the hoop (transverse) direction. Column C3 was retrofitted with four layers of CFRP sheets, comprising two layers in the hoop (transverse) direction and two layers in the longitudinal direction.

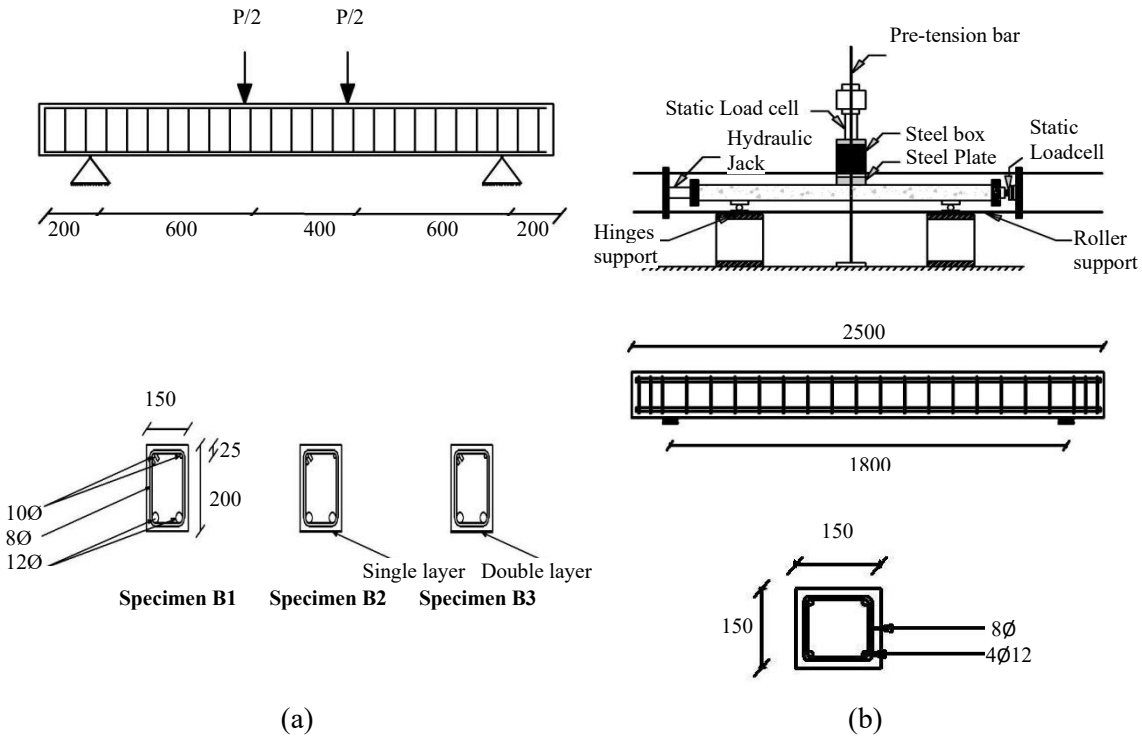


Figure 1: (a) Beam specimen adapted from Esfahania et al. (2006) and (b) column specimen adapted from Alaa et al. (2022**)**.

Similar CFRP-strengthened beam and column models, along with the corresponding loading conditions, are simulated using SAP2000. The load–deflection curves obtained from the experimental tests and the numerical simulations are presented in Figure 2. Comparisons of the ultimate load and the corresponding deflection for the three beam specimens and three column specimens are presented in Tables 2 and 3 respectively. The numerical results show good agreement with the experimental results in terms of key response parameters, including the yield load, ultimate load and load–deflection behaviour. The variation in the predicted ultimate load ranges from 0.89% to 10.66%, while the variation in the corresponding ultimate deflection ranges from 6.93% to 14.52%.

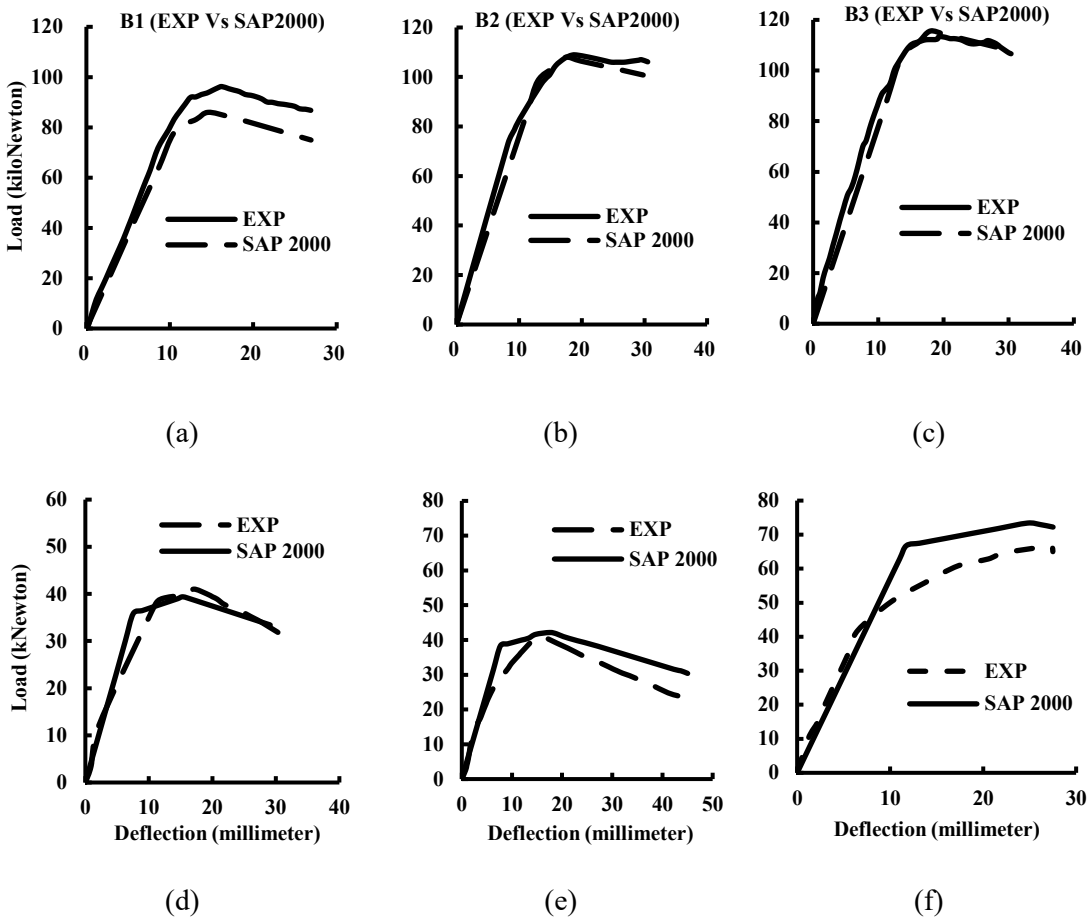


Figure 2: (a) Specimen B1, (b) Specimen B2, (c) Specimen B3, (d) Control specimen, (e) specimen strengthened with one horizontal layer and (f) specimen strengthened with two longitudinal and two horizontal layers

Table 2: Beam samples - Experimental (Esfahania et al., 2006) vs. Simulated (SAP2000) model

Sample	Particulars	Experimental	Simulated	% Difference
B1 (Control specimen)	Ultimate Load (kiloNewton)	96.24	85.98	10.66
	Deflection (millimeter)	16.24	14.58	10.22
B2 (Single layer)	Ultimate Load (kiloNewton)	108.91	107.94	0.89
	Deflection (millimeter)	19.14	17.39	9.14
B3 (Double layer)	Ultimate Load (kiloNewton)	113.41	115.62	1.95
	Deflection (millimeter)	19.35	18.01	6.93

Table 3: Column samples - Experimental (Alaa et al., 2022) *vs.* Simulated (SAP2000) model

Sample	Axial Load (kiloNewton)	Particulars	Experimental	Simulated	% Difference
Control specimen	144	Ultimate Load (kiloNewton)	41.01	39.38	10.12
		Deflection (millimeter)	17.10	15.37	3.97
SS 1 horizontal layer	145	Ultimate Load (kiloNewton)	40.92	42.15	14.52
		Deflection (millimeter)	15.29	17.51	3.01
SS 2L-2H layer	146	Ultimate Load (kiloNewton)	66.53	73.40	9.13
		Deflection (millimeter)	27.26	24.77	10.33

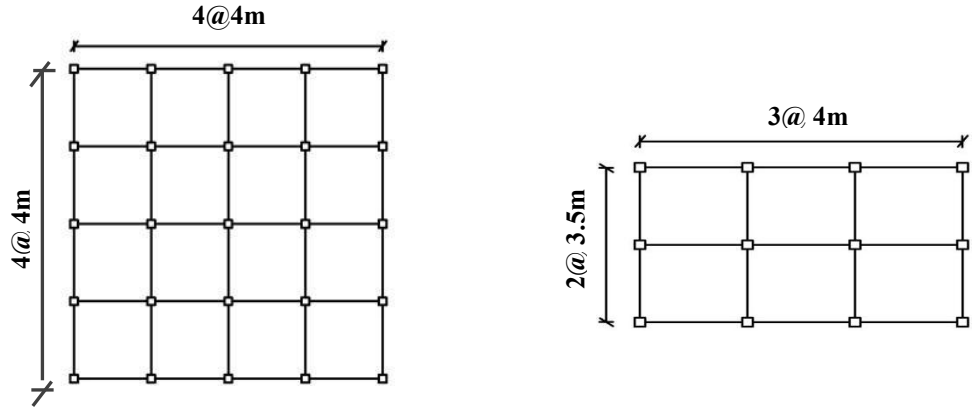
The comparison demonstrates that the adopted SAP2000 model accurately captures the structural response, with differences of less than 15% from the reference results. Accordingly,

the model is deemed suitable for performing parametric studies on beams and columns strengthened with UHM-CFRP panels.

3. Methodology

3.1 Structural Model

In this study, two different building plans; plan-A and plan-B are considered. Plan-A buildings (Figure 3a) are used in the initial stages of the study (Sections 3 and 4), whereas plan-B buildings (Figure 3b) are used for the validation stage (Section 5). The plan-A buildings have the identical floor plan dimensions, consisting of four bays with a span length of 4 m in each of the two orthogonal (X and Y) directions and a uniform storey height of 3.3 meters. Four building height configurations are considered: 4-, 6-, 8- and 10-storey buildings. The structural members are designed using M25 grade concrete and Fe415 rebar steel. The buildings are initially designed to satisfy an IDR limit of 2%, and their seismic performance is evaluated through NLTHA using five SCGMs listed in Table 5. These M25-grade building models are considered as the baseline (reference) models. To investigate the influence of material deterioration, the concrete grade is systematically reduced to M20, M15 and M10, representing successive groups of building models. This approach is based on the premise that buildings originally designed with a specified concrete grade may experience a reduction in concrete strength over time due to ageing, deterioration or other adverse effects. The UHM CFRP wrapping is subsequently adopted as a retrofitting measure for these deteriorated building models. The material properties of the UHM CFRP used for strengthening are presented in Table 4. The UHM CFRP strengthening is modelled for the structural members of each concrete strength group. All building models are developed, designed and analysed using SAP2000.



(a) (b)

Figure 3: Building layouts: (a) Plan-A and (b) Plan-B

202

Table 4: Physical properties of UHM CFRP used in modelling (Adopted from Akram et al. (2021))

Symbol	Definition	Value	Unit
E_x	Longitudinal elastic modulus	514	GigaPascal
E_y ,E_x	Transverse elastic-modulus	10	GigaPascal
G_{xz}, G_{xy}	In-plane shear modulus	6	GigaPascal
G_{yz}	out-plane shear modulus	3.6	GigaPascal
μ_{xy}, μ_{xz}	In-plane Poison's ratio	0.26	
μ_{yz}	Out-plane Poison's ratio	0.3	
γ	Density	1820	Kilogram per cu.meter
t	Thickness	1	millimeter
f_{fu}	Ultimate tensile strength	1923	GigaPascal
ε_{fu}	Ultimate strain	1.6	%

203

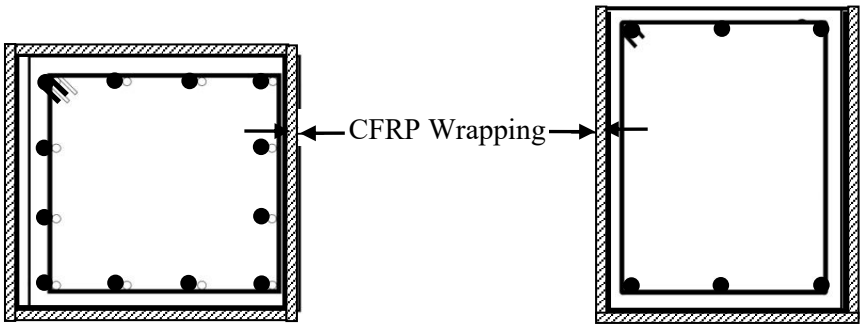


Figure 4: Illustration of typical CFRP wrapping; (a) Column - Full and (b) Beam - U.

204

205 The CFRP wrapping configurations considered for columns and beams are Full wrapping and
206 U-wrapping as shown in Figures 4(a) and 4(b) respectively. The columns are fully wrapped
207 with CFRP to enhance their lateral load-carrying capacity and beams are U-wrapped with
208 CFRP to improve their ductility. A single layer of 1 millimeter thick CFRP wraps are applied
209 to both column and beam. The beam and column sections are modeled with lumped plastic
210 hinges, whose nonlinear properties are defined using moment–curvature characteristics of the
211 respective RC sections. As stipulated in ACI 440.2R-17, the plastic hinge length for beams
212 may be estimated as two times the overall member depth. Alternatively, this length can be

evaluated through a more detailed analytical assessment, provided that the resulting value is not taken as less than the beam's depth. For columns, jacketed with CFRP, the plastic hinge length (L_p) is calculated using Equation (1).

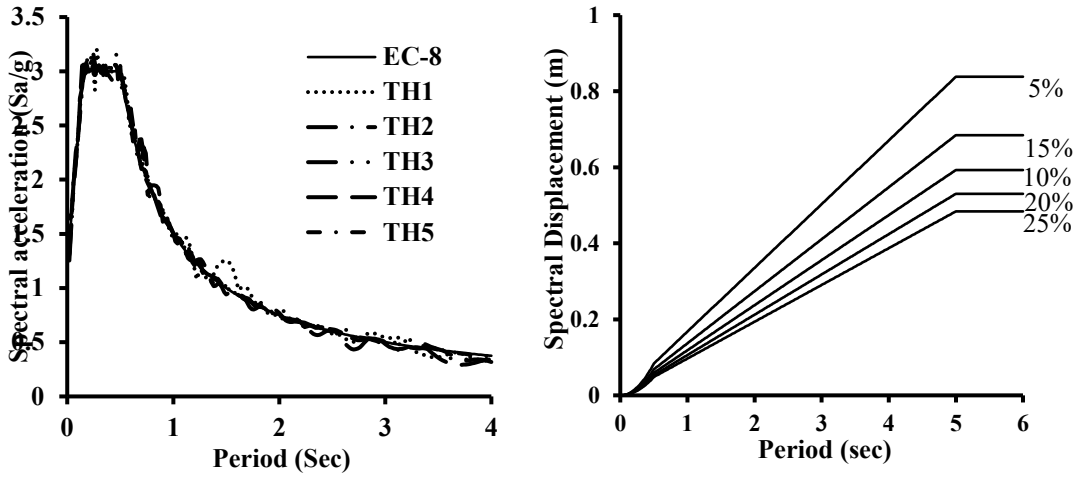
$$L_p = g + 0.044 f_y d_{b1} \quad (1)$$

In Equation (1), d_{b1} and f_y represent the diameter and yield strength of the longitudinal steel reinforcement respectively. The variable g represents the clear gap between the FRP jacket and any adjacent structural members. g must not exceed 50.8 mm.

Table 5: Details of spectrum compatible ground motions (PEER Database)

Sl. No.	Name	Background Earthquake	Record No.	Duration (seconds)
1	TH-1	Duzce 1999	Duzce, 270 (ERD)	25.9
2	TH-2	El Centro 1940	N-S Component	31.8
3	TH-3	Gazli 1976	Karakyr, 090	16.3
4	TH-4	Kocaeli 1999	Sakarya, 090 (ERD)	60.0
5	TH-5	N. Palm Spring 1986	0920, USGS station 5070	20.0

The Spectrum-Compatible Ground Motions (SCGMs) listed in Table 5 are generated using the software developed by Kumar (2004**)**. The generated SCGMs incorporate the phase angle, frequency content and duration characteristics of the background earthquake. Figure 5(a) compares the design acceleration spectrum *Eurocode 8 (Part 1):(2013)* with the SCGM response spectrum, for a Peak Ground Acceleration (PGA) of 0.45g and a damping ratio of 5%. The corresponding design displacement spectrum is presented in Figure 5(b). For the Nonlinear Time-History Analyses (NLTHA), the effective member section properties are adopted in accordance with *IS 1893 (Part 1): (2016*).



(a) (b)

Figure 5: (a) Design acceleration spectrum and SCGM Response spectrum match, (b) Design displacement spectrum

230

231 **3.2 Design Procedure**

232 The seismic design lateral loads are determined using the Direct Displacement-Based Design
233 (DDBD) methodology. The design objectives are established by controlling the inter-storey
234 drift limits to ensure that the structural members satisfied the specified performance levels.
235 Based on these design objectives, the allowable range of beam depths are determined in
236 accordance with Choudhury and Singh (2013), while the column dimensions are adopted
237 following Choudhury and Singh (2013). The nomenclature of the building configurations and
238 the corresponding structural member sizes are presented in Table 6.

239

240

241

242

243

244

245

246

247

248

Table 6: Nomenclature and member sizes for plan-A buildings

Model	Description	Beam (meter × meter)	Columns storey-wise (meter)									
			1st	2nd	3rd	4th	5th	6th	7th	8th	9th	10th
N4M25	4 storey M25	0.25×0.45	0.375	0.36	0.355	0.35						
N4M20	4 storey M20											
N4M15	4 storey M15											
N4M10	4 storey M10											
F4M25	4 storey M25+ FRP											
F4M20	4 storey M20 + FRP											
F4M15	4 storey M15 + FRP											
F4M10	4 storey M10 + FRP											
N6M25	6 storey M25	0.3×0.45	0.54	0.52	0.50	0.48	0.44	0.43				
N6M20	6 storey M20											
N6M15	6 storey M15											
N6M10	6 storey M10											
F6M25	6 storey M25 + FRP											
F6M20	6 storey M20 + FRP											
F6M15	6 storey M15 + FRP											
F6M10	6 storey M10 + FRP											
N8M25	8 storey M25	0.3×0.45	0.58	0.535	0.50	0.48	0.46	0.45	0.43	0.43		
N8M20	8 storey M20											
N8M15	8 storey M15											
N8M10	8 storey M10											
F8M25	8 storey M25 + FRP											
F8M20	8 storey M20 + FRP											
F8M15	8 storey M15 + FRP											
F8M10	8 storey M10 + FRP											
N10M25	10 storey M25	0.3×0.45	0.65	0.63	0.60	0.57	0.55	0.53	0.50	0.47	0.45	0.42
N10M20	10 storey M20											
N10M15	10 storey M15											
N10M10	10 storey M10											
F10M25	10 storey M25 + FRP											
F10M20	10 storey M20 + FRP											
F10M15	10 storey M15 + FRP											
F10M10	10 storey M10 + FRP											

249 The longitudinal steel rebar reinforcement ratio is maintained between approximately 0.8%
250 and 4% of the gross cross-sectional area of the columns. The corresponding building design
251 parameters are presented in Table 7.

252 **Table 7: Design parameters for plan-A buildings (Priestley, 2007)**

	4 storey	6 storey	8 storey	10 storey
Design IDR (%)	2	2	2	2
Effective mass (kilogram)	9,95,762	19,27,865	23,14,864	29,79,767
Effective height (meter)	9.24	13.07	17.37	21.47
Design displacement (millimeter)	184.72	221.92	291.503761	358.64
Equivalent damping (Newton-seconds per meter)	13.18	11.88	11.53	11.46
Effective period (second)	1.49	1.88	2.23	2.75
Base shear (kiloNewton)	3273.52	4782.75	5361.29	5583.27

253

254 **4. Results and Discussion**

255 **4.1 IDR**

256 After the Plan-A building models are designed in accordance with the procedures described in
257 Section 3, NLTHA are performed using the five SCGMs listed in Table 5. The resulting
258 response parameters are analysed to evaluate the dynamic behaviour of the building models.
259 Figures 6, 7, 8 and 9 show the IDR profiles of the 4-, 6-, 8- and 10-storey Plan-A building
260 models before and after CFRP strengthening. The figures show that the CFRP-strengthened
261 building models consistently exhibit lower IDRs than the corresponding unstrengthened
262 models, indicating an improvement in seismic performance.

263 The IDR results indicate that CFRP strengthening significantly enhances the seismic
264 performance of RC frame buildings, with the level of improvement depending on both the
265 building height and the concrete grade. Among the investigated building models, the 4-storey
266 buildings exhibit the greatest benefit, particularly for lower concrete grades. The maximum
267 IDR of the unstrengthened models increase from 2.95% for the M25-grade building to 3.55%
268 for the M10-grade building. Following CFRP strengthening, the corresponding maximum
269 IDRs decreased to 1.92% and 2.80% respectively, indicating a substantial reduction in
270 seismic demand. Relative to the corresponding unstrengthened building models, the
271 maximum IDR decreased by 31.5%, 26.6% and 21.2% for the M20-, M15- and M10-grade
272 buildings respectively.

273

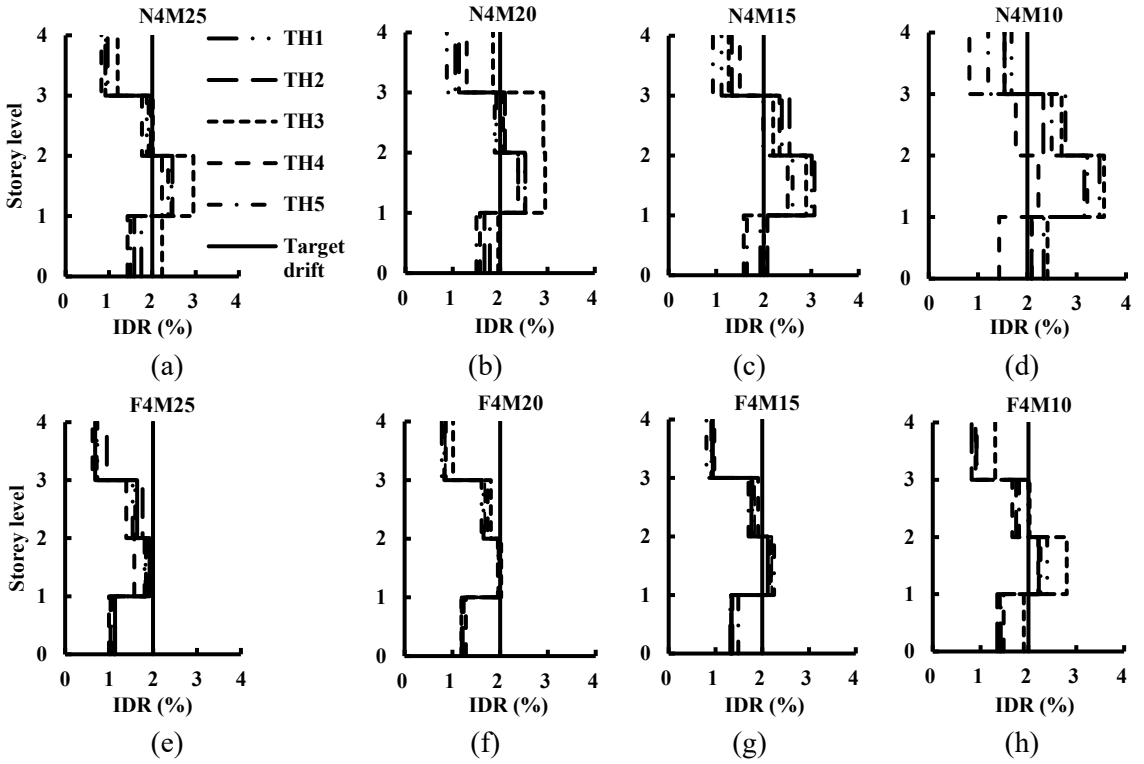


Figure 6: IDR profiles along the building height for Plan-A 4-storey buildings corresponding to 2% target IDR.

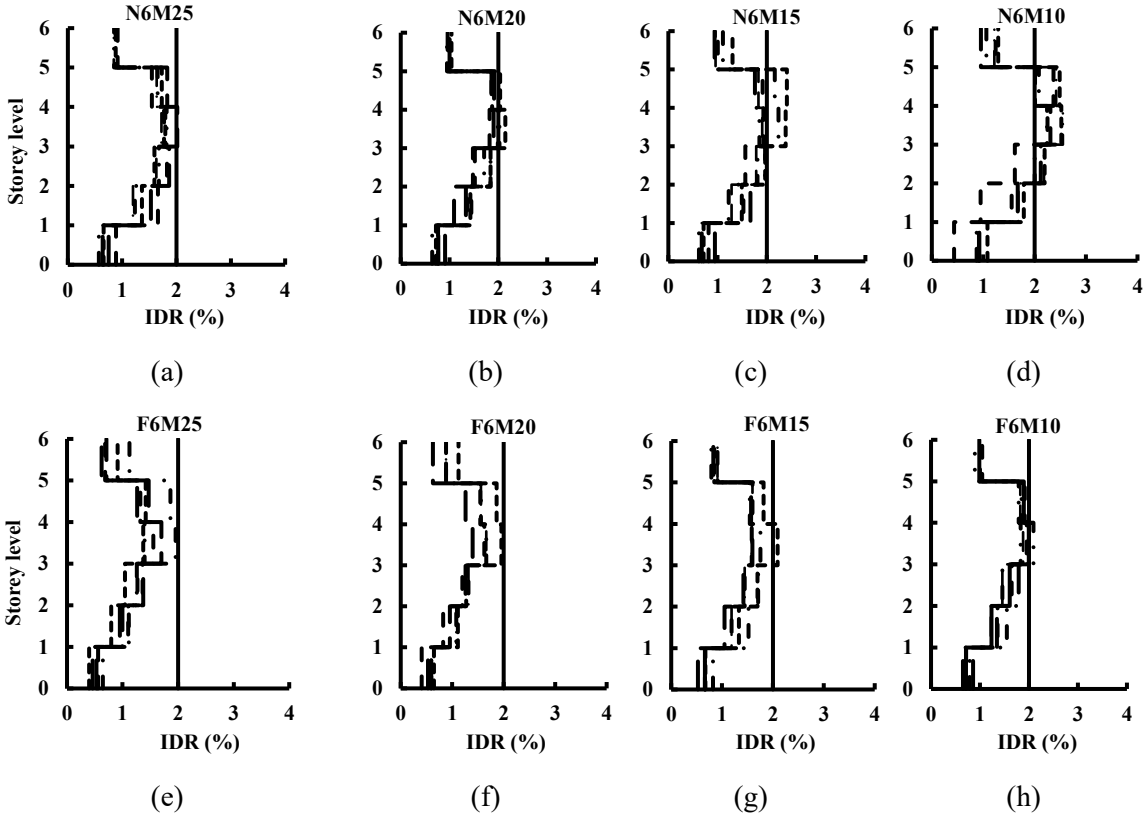


Figure 7: IDR profiles along the building height for Plan-A 6-storey buildings corresponding to 2% target IDR.

For the 6-storey building models, the effectiveness of CFRP strengthening becomes more evident as the concrete grade decreases. The maximum IDR of the unstrengthened M10-grade building reduces from 2.55% to 2.09% following CFRP strengthening, corresponding to a reduction of 17.5%.

A similar trend is observed for the 8-storey building models. The CFRP-strengthened M15- and M10-grade buildings exhibit reductions in maximum IDR of 17.36% and 17.24% respectively, resulting in seismic performance comparable to that of the unstrengthened M20-grade building models.

For the 10-storey building models, CFRP strengthening reduces the maximum IDR by 16.97%, 10.28%, 7.94% and 7.94% for the M25-, M20-, M15- and M10-grade buildings respectively. Overall, the results demonstrate that CFRP strengthening consistently reduces the inter-storey drift ratio across all investigated building heights and concrete grades. Although the magnitude of improvement varies with building height and concrete grade. The observed reductions in IDR confirm the effectiveness of CFRP strengthening as a retrofit strategy for enhancing the seismic performance of RC frame buildings.

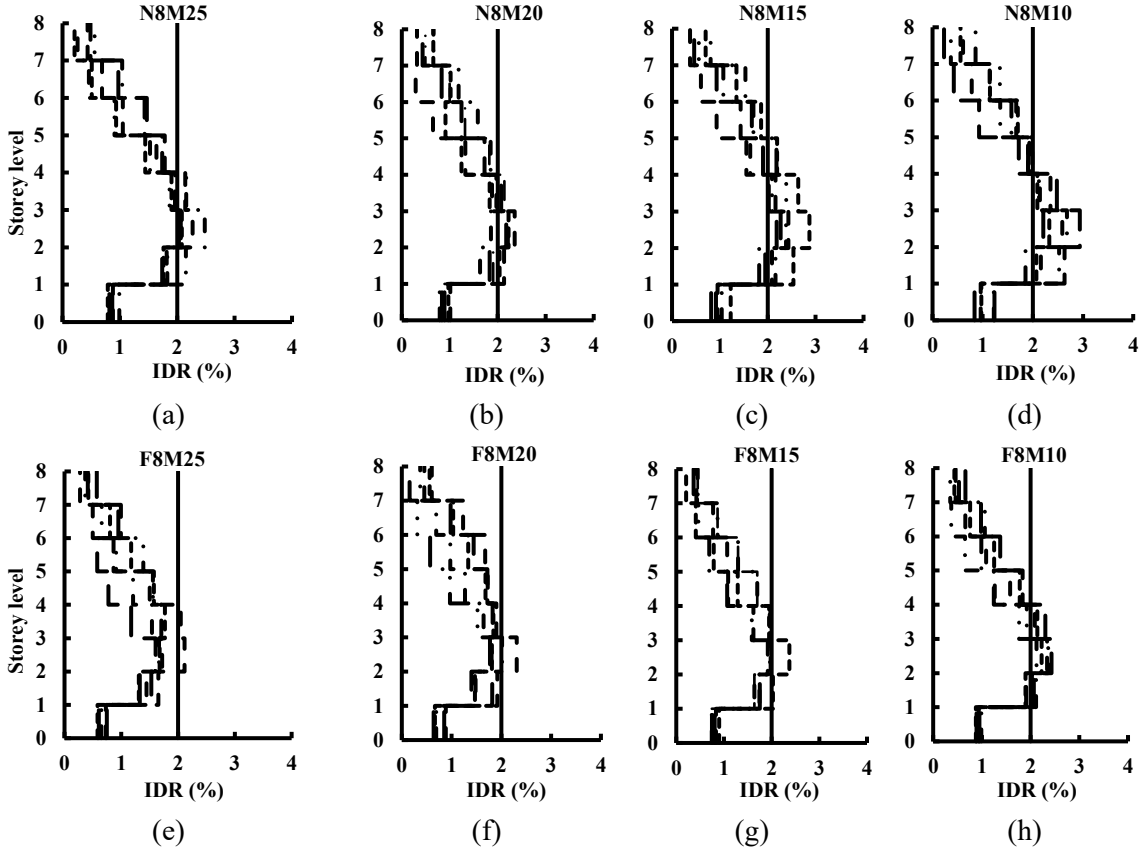


Figure 8: IDR profiles along the building height for Plan-A 8-storey buildings corresponding to 2% target IDR.

290

291

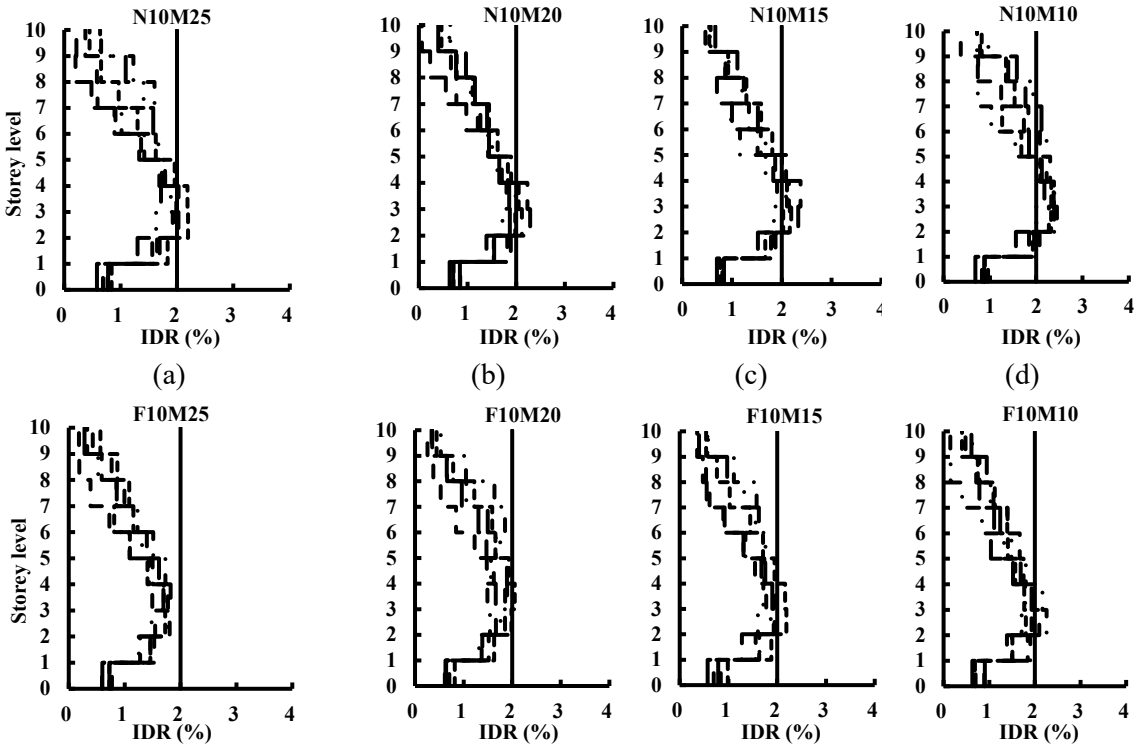


Figure 9: IDR profiles along the building height for Plan-A 10-storey buildings corresponding to 2% target IDR.

292

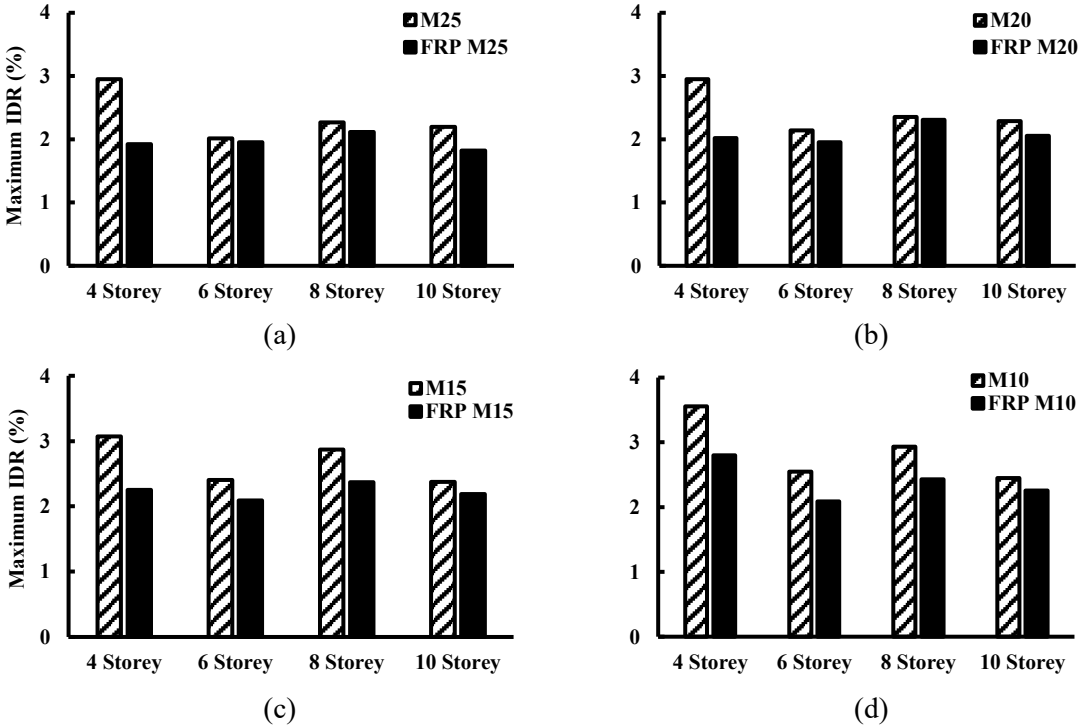
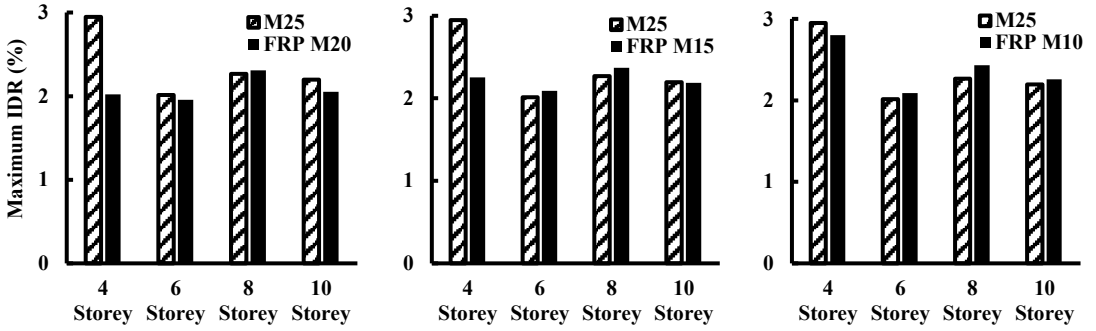


Figure 10: Variation of maximum IDR with building height for unstrengthened and CFRP-strengthened buildings: (a) M25, (b) M20, (c) M15 and (d) M10

Figure 10 presents the maximum IDR obtained from NLTHA of the 4-, 6-, 8- and 10-storey building models, with each model subjected to a suite of five SCGMs. The maximum IDRs of the unstrengthened M25-grade building models are compared with those of the corresponding CFRP-strengthened M25-, M20-, M15- and M10-grade building models. As shown in Figure 10(a)–(d), the CFRP-strengthened M20-, M15- and M10-grade building models consistently exhibit lower maximum IDRs than the corresponding unstrengthened M25-grade building models, indicating the effectiveness of CFRP strengthening in enhancing the seismic performance of RC frame buildings constructed with low-strength concrete and existing RC buildings with deteriorated concrete strength.



(a) (b) (c)

Figure 11: Variation of maximum IDR with building height between the unstrengthened M25 and CFRP-strengthened buildings: (a) M25 *Vs.* CFRP-strengthened M20, (b) M25 *Vs.* CFRP-strengthened M15 and (c) M25 *Vs.* CFRP-strengthened M10.

As shown in Figure 11, CFRP strengthening substantially reduces IDR response of the M20-, M15- and M10-grade building models, bringing their seismic response closer to that of the corresponding unstrengthened M25-grade building models. Except for the 4-storey buildings, the differences in the maximum IDR between the CFRP-strengthened M20-, M15- and M10-grade buildings and the corresponding unstrengthened M25-grade buildings are approximately 34.82%, 31.48%, and 23.61% respectively.

4.2 IDR ratio relation with concrete grade

The maximum IDR values of the building models with and without CFRP strengthening are obtained from five NLTHA conducted for each building model. Figure 12 illustrates the variation of the average IDR ratio with concrete grade. Equations (2)–(5) represent the linear trendline equations relating the average IDR ratio of the CFRP-strengthened building models to that of the corresponding unstrengthened building models for the 4-, 6-, 8- and 10-storey buildings respectively. The baseline in the figure represents the average IDR ratio of the

unstrengthened building models. These equations are subsequently combined to develop the generalized predictive equation given as Equation (6). This equation can be used to estimate the average IDR ratio for RC frame buildings with different concrete grades and building heights.

$$I_4 = 0.753 + 0.00085M \quad (2)$$

$$I_6 = 0.797 + 0.00085M \quad (3)$$

$$I_8 = 0.842 + 0.00085M \quad (4)$$

$$I_{10} = 0.886 + 0.00085M \quad (5)$$

$$I_n = 0.665 + 0.02213n + 0.00085M \quad (6)$$

Where, I_n represent the average IDR ratio of buildings with CFRP strengthened buildings relative to that of the corresponding unstrengthened buildings, M represents the concrete grade and n represents the number of storeys.

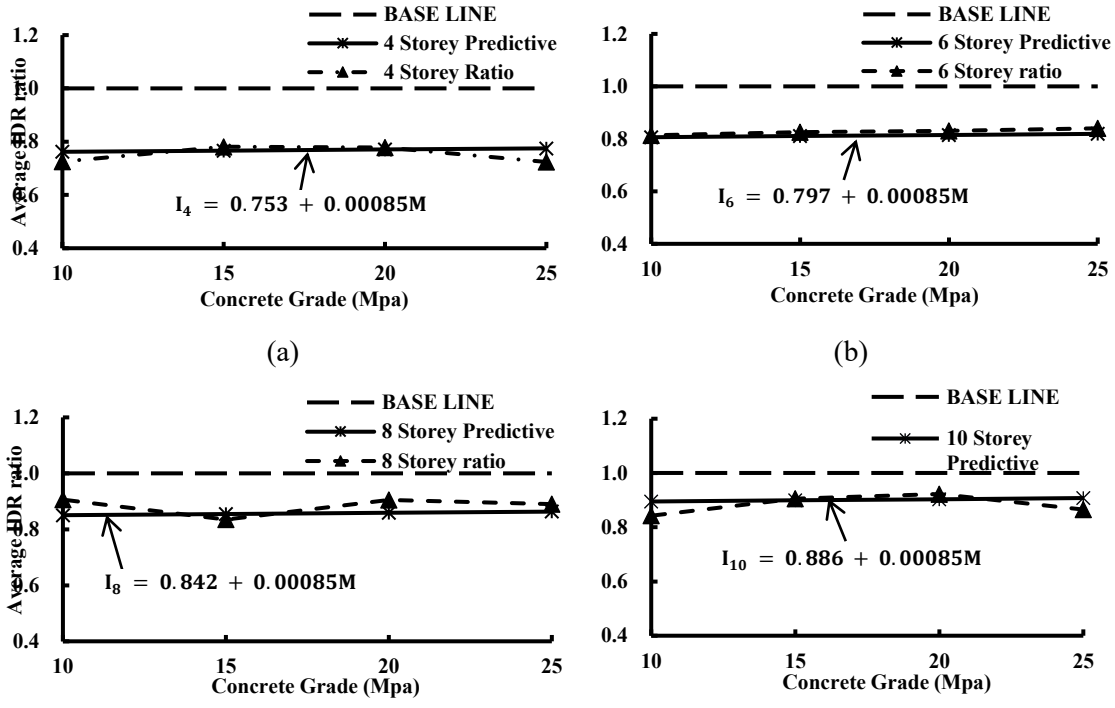


Figure 12: Average IDR ratio *Vs.* Concrete Grade

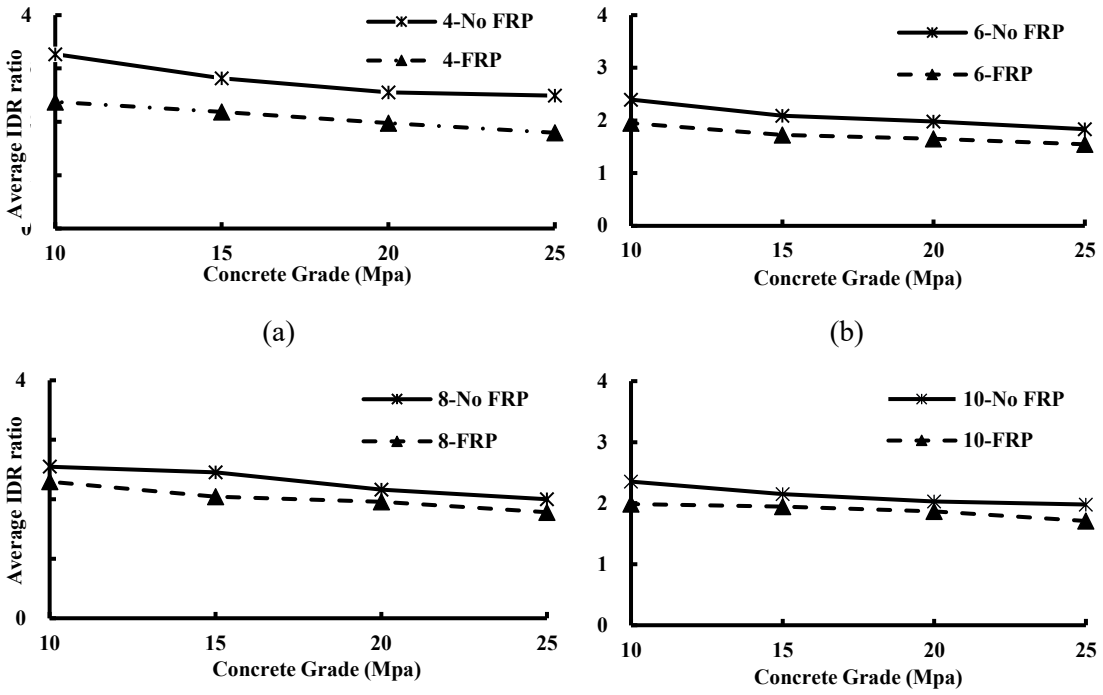


Figure 13: Average IDR (%) *Vs*. Concrete Grade (*MPa*)

Figure 13 shows the comparison of average IDRs obtained from five time-history records for different concrete grades, with and without CFRP. Significant reductions in IDR are observed in all the building models.

4.3 Stiffness

Figure 14 shows the maximum stiffness obtained from NLTHA using five SCGMs for the 4-, 6-, 8- and 10-storey building models. The maximum stiffness of the unstrengthened M25-grade building models are compared with those of the CFRP strengthened M25-, M20-, M15- and M10-grade building models. For the M25-grade buildings, CFRP strengthening increased the maximum stiffness by 27.06%, 42.20%, 50.06% and 15.17% for the 4-, 6-, 8- and 10-storey buildings respectively. For the M20-grade buildings, the corresponding increases are 30.68%, 28.84%, 32.45%, and 17.05% respectively. Similarly, the stiffness increase by 51.46%, 16.41%, 40.01% and 28.73% respectively for the CFRP-strengthened M15-grade buildings. For the M10 concrete buildings, the corresponding increments are 40.52%, 17.38%, 45.77% and 42.29% respectively. These results indicate that CFRP strengthening

substantially enhances the lateral stiffness of RC frame buildings across all investigated concrete grades and building heights.

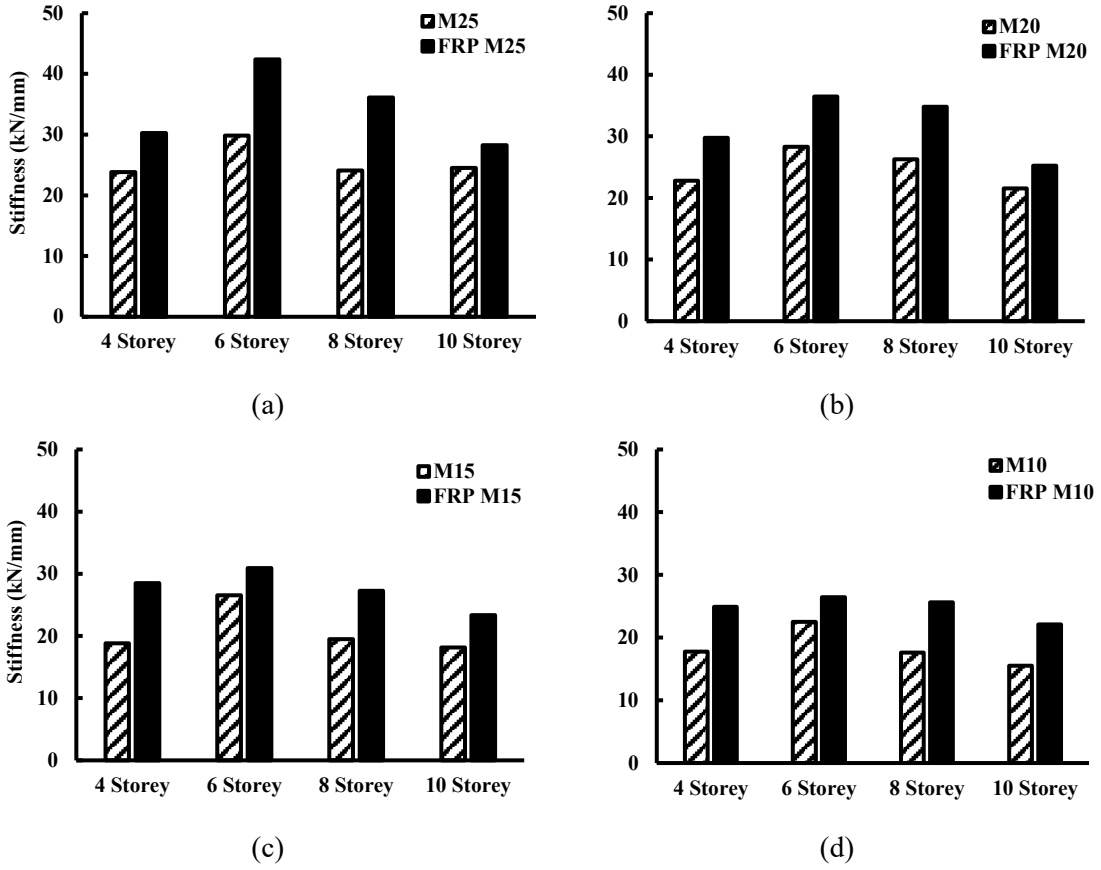
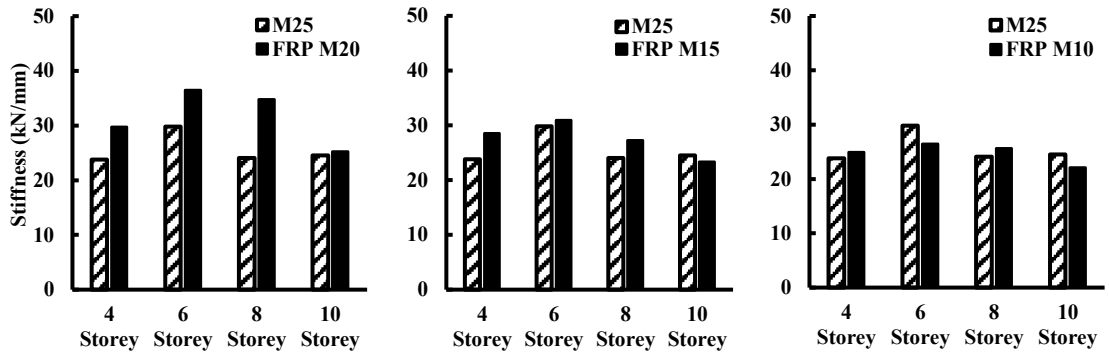


Figure 14: Stiffness variation with building height for unstrengthened and CFRP-strengthened buildings: (a) M25, (b) M20, (c) M15 and (d) M10.

Figure 15 compares the stiffness of the M25 building models without CFRP wrapping with those of the M20, M15 and M10 building models strengthened with CFRP wrapping. Compare with the CFRP-strengthened M20 building models, the stiffness increase by 25.07%, 22.34%, 44.52% and 2.91% for the 4-, 6-, 8- and 10-storey buildings respectively. For the CFRP-strengthened M15 building models, the stiffness increase by 19.82%, 3.71% and 13.36% for the 4-, 6- and 8-storey buildings respectively. Whereas, the stiffness of the CFRP-strengthened 10-storey building is 4.71% lower than that of the corresponding M25 building model without CFRP wrapping. For the CFRP-strengthened M10 building models, the stiffness increase by 4.72% and 6.53% for the 4- and 8-storey buildings respectively. Whereas the stiffness of the 6- and 10-storey buildings are 11.37% and 9.86% lower respectively, than that of the corresponding M25 building models without CFRP wrapping.



(a) (b) (c)

Figure 15: Stiffness variation with building height between the unstrengthened M25 and CFRP-strengthened buildings: (a) M25 Vs. CFRP-strengthened M20, (b) M25 Vs. CFRP-strengthened M15 and (c) M25 Vs. CFRP-strengthened M10.

361

362 **4.4 Building stiffness ratio relation with concrete grade**

363 Table 8 presents the maximum stiffness values of the buildings before and after CFRP
364 treatment, obtained from five NLTHA conducted for each building model. The improvement
365 in stiffness is quantified using the building stiffness ratio, defined as the ratio of the stiffness
366 before CFRP strengthening to that after CFRP strengthening. The results indicate that CFRP
367 strengthening significantly enhances both the stiffness of individual structural members and
368 the overall lateral stiffness of the buildings. To quantify and generalize this improvement,
369 predictive equations were developed to estimate the building stiffness ratio as a function of
370 concrete grade and building height. Equations (7), (8), (9) and (10) represent the trendline
371 equations for the 4-, 6-, 8-, and 10-storey building models respectively, relating the building

372 **Table 8: Maximum building stiffness ratio**

	Grade	Stiffness (kiloNewton/millimeter)		Building stiffness ratio
		without FRP	with FRP	
4 storey	**M25**	23.80	29.76	0.80
	M20	22.78	29.77	0.77
	M15	18.83	28.52	0.66
	M10	17.74	24.93	0.71
6 storey	**M25**	29.8	42.4	0.70
	M20	28.32	36.48	0.78
	M15	26.56	30.93	0.86
	M10	22.52	26.43	0.85
8 storey	**M25**	24.07	36.12	0.67
	M20	26.26	34.78	0.76
	M15	19.48	27.28	0.71
	M10	17.59	25.64	0.69
10 storey	**M25**	24.53	28.25	0.87
	M20	21.56	25.24	0.85
	M15	18.15	23.37	0.78
	M10	15.54	22.11	0.70

373

374 stiffness ratio to the concrete grade. Equation (11) presents a generalized predictive equation
375 applicable to all building models, relating the building stiffness ratio to both the concrete
376 grade and the number of storeys. The corresponding relationships are illustrated in Figure 16.

$$K_4 = 0.733 + 0.010775M - 0.000375M^2 \quad (7)$$

$$K_6 = 0.729 + 0.010775M - 0.000375M^2 \quad (8)$$

$$K_8 = 0.694 + 0.010775M - 0.000375M^2 \quad (9)$$

$$K_{10} = 0.628 + 0.010775M - 0.000375M^2 \quad (10)$$

$$K_n = 0.648 + 0.03706n - 0.003906n^2 + 0.010775M - 0.000375M^2 \quad (11)$$

377

Where K_n represents the average building stiffness ratio of an n storey building without CFRP wrapping to that of the corresponding building with CFRP wrapping, M represents the concrete grade, and n represents the storey level.

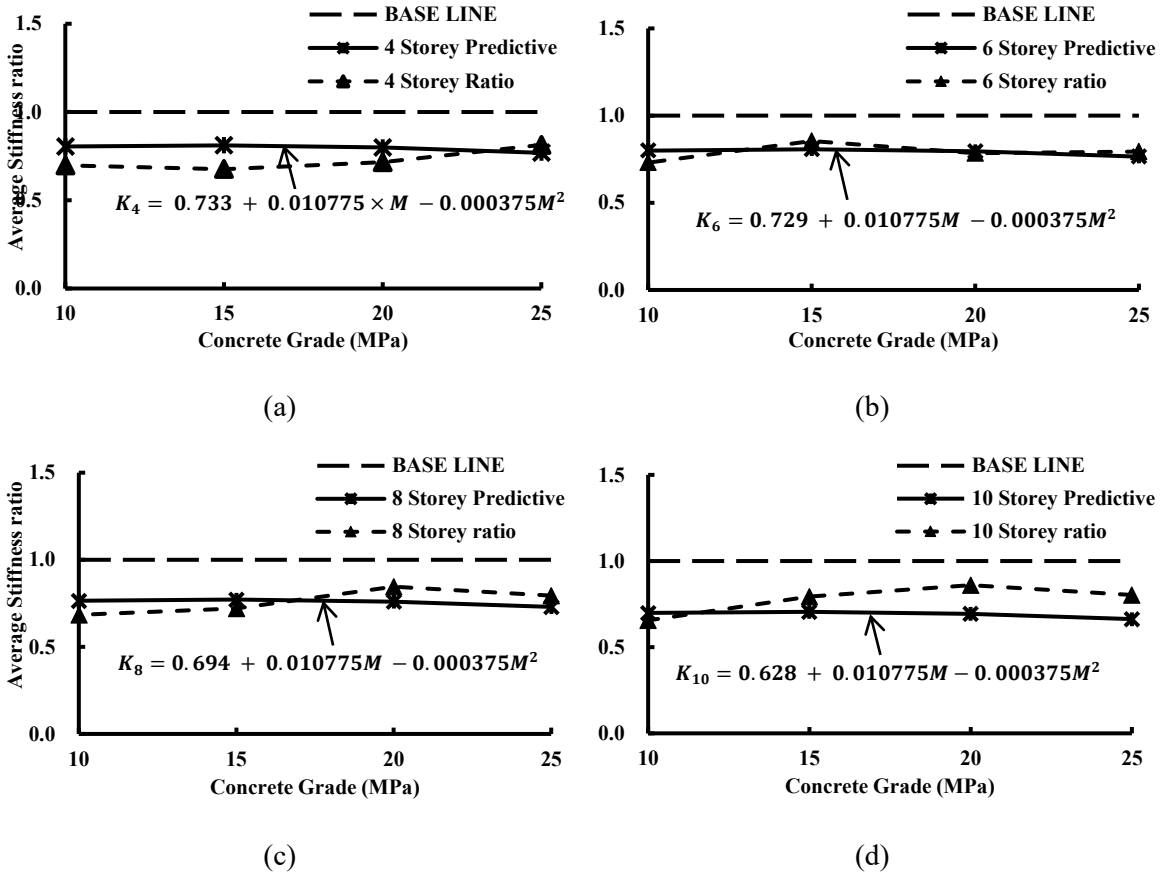


Figure 16: Average Building stiffness ratio *Vs.* Concrete Grade (MPa)

Following CFRP strengthening, as described in Section 3, Equation (11) can be used to predict the building stiffness ratio and, consequently, the expected increase in the overall stiffness of the building. For concrete grades not explicitly analysed, such as M11, M12, M13, M14, M16, M17, and M18, the corresponding building stiffness ratios can be estimated using this equation. This approach enables the estimation of the building stiffness ratio for any intermediate concrete grade with reasonable accuracy. Figure 17 compares the average stiffness values calculated from NLTHA using five earthquake ground-motion records for buildings of different concrete grades, with and without CFRP strengthening. A significant increase in stiffness is observed for all CFRP-strengthened building models relative to their unstrengthened counterparts.

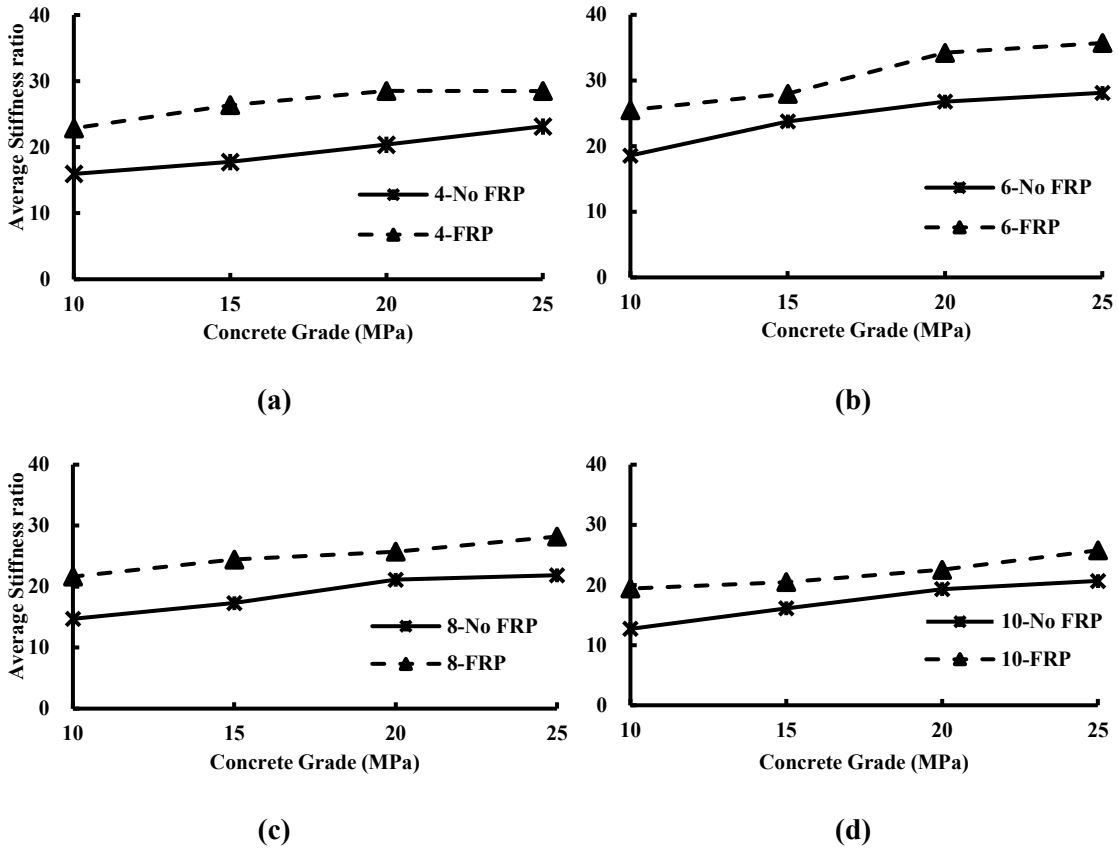


Figure 17: Average Stiffness (kN/m) *Vs.* Concrete Grade (MPa)

392

393 **5. Validation**

394 In this section, Equations (6) and (11) are validated using building models with different plan
395 configurations (Plan B, Figure 3b) and heights (5-storey and 7-storey). The analysis and
396 design of both building models were performed following the methodology described in
397 Section 3. A new set of six earthquake ground-motion records given in Table 9 was selected
398 instead of those used in the previous analysis. All selected ground-motion records were scaled
399 to be compatible with a peak ground acceleration of 0.45 g and 5% damping as shown in
400 Figure 18. The design parameters are given in Table 10. Nomenclature and structural member
401 sizes are given in Table 11.

402

403

404

405

Table 9: Details of spectrum compatible ground motions (PEER Database)

Sl. No.	Name	Background Earthquake	Record No.	Duration (seconds)
1	TH-6	Northern California 1954	Ferndale City Hall	40
2	TH-7	El Alamo Earthquake 1954	El Centro Array	60
3	TH-8	Borrego Mountain Earthquake 1968	El Centro Array	79.9
4	TH-9	Imperial Valley earthquake 1979	Holtville Post Office / Imperial Valley Station	35.08
5	TH-10	Victoria, Mexico Earthquake 1980	SAHOP Casa Flores, Mexicali	15.74
6	TH-11	Coalinga Earthquake 1983	Parkfield / CAK Station	50

406 .

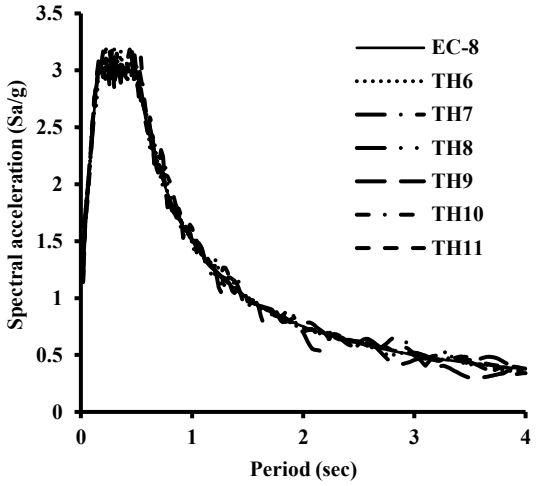


Figure 18: Design acceleration spectrum and SCGM response spectrum match.

407

408 **Table 10: Design parameters of plan-B buildings (Priestley, 2007)**

	5 storey		7 storey	
	X-direction	**Y-direction**	**X-direction**	**Y-direction**
Design IDR (%)	0.02	0.02	0.02	0.02
Effective mass (kilogram)	5,11,750.39	5,11,750.39	7,56,550.02	7,56,550.02
Effective height (meter)	11.04	11.04	15.32	15.32
Design displacement (millimeter)	188.27	188.27	257.83	257.83
Equivalent damping (Newton-seconds per meter)	11.06	13.1	11.57	13.6
Effective period (seconds)	1.57	1.73	2.18	2.31
Base shear (kiloNewton)	1544.42	1271.95	1621.69	1444.30

409

Table 11: Nomenclature and member sizes for plan-B buildings

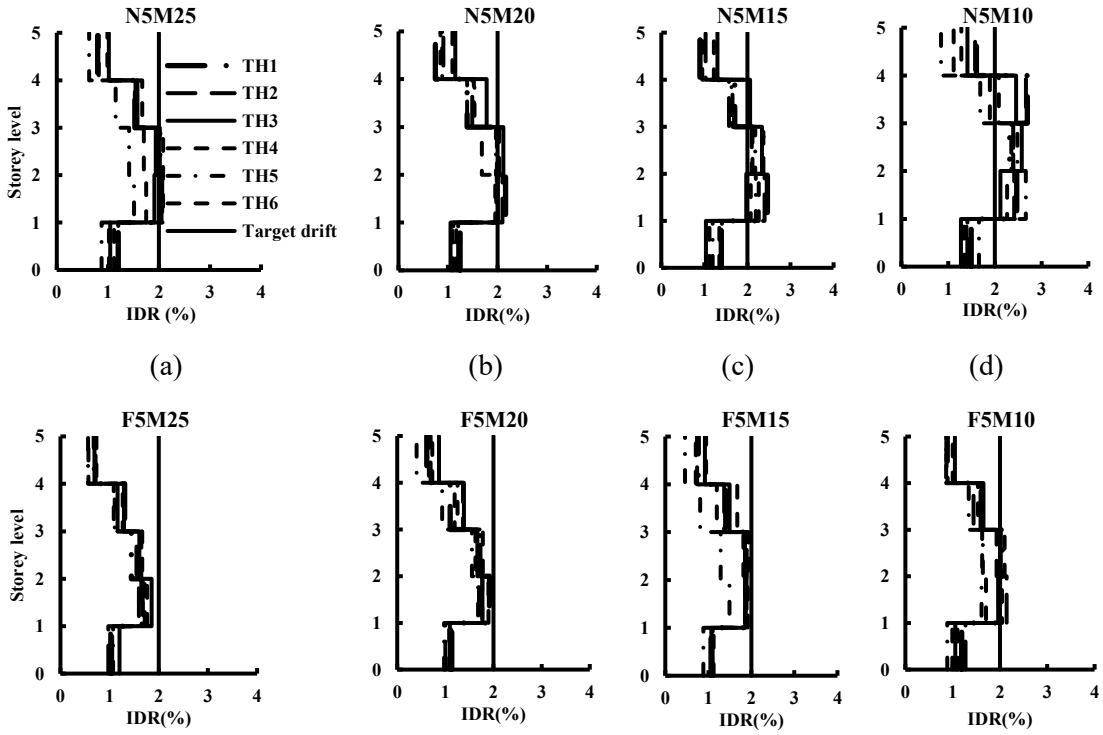
Model	**Description**	**Beam (meter×meter)**	**Column storey wise (meter)**						
			1st	**2nd**	**3rd**	**4th**	**5th**	**6th**	**7th**
N5M25	5 storey M25	0.25 × 0.43	0.44 × 0.46	0.43 × 0.44	0.41 × 0.42	0.39 × 0.4	0.37 × 0.38	-	-
N5M20	5 storey M20								
N5M15	5 storey M15								
N5M10	5 storey M10								
F5M25	5 storey M25 + FRP								
F5M20	5 storey M20 + FRP								
F5M15	5 storey M15 + FRP								
F5M10	5 storey M10 + FRP								
N7M25	7 storey M25	0.25 × 0.45	0.54 × 0.56	0.51 × 0.54	0.48 × 0.51	0.45 × 0.48	0.43 × 0.45	0.4 × 0.43	0.38 × 0.41
N7M20	7 storey M20								
N7M15	7 storey M15								
N7M10	7 storey M10								
F7M25	7 storey M25 + FRP								
F7M20	7 storey M20 + FRP								

F7M15	7 storey M15 + FRP
F7M10	5 storey M10 + FRP

Figures (19)–(20) present the inter-storey drift ratio (IDR) profiles along the storey height for the CFRP-strengthened and unstrengthened 5-storey buildings in the two orthogonal directions (X and Y).

In the X-direction, the maximum IDR for the unstrengthened M10-grade concrete building is 2.7%, which decreases to 2.1% after CFRP strengthening. For the M15-grade building, the maximum IDR decreases from 2.5% in the unstrengthened condition to 2.0% in the CFRP-strengthened condition. Similarly, the maximum IDR decreases from 2.2% to 1.9% for the M20-grade building and from 2.1% to 1.9% for the M25-grade building.

In the Y-direction, the maximum IDR for the unstrengthened M10-grade concrete building is 2.7%, which decreases to 2.2% after CFRP strengthening. For the M15-grade building, the maximum IDR decreases from 2.5% in the unstrengthened condition to 1.9% in the CFRP-strengthened condition. Similarly, the maximum IDR decreases from 2.2% to 1.8% for the M20-grade building and from 2.1% to 1.8% for the M25-grade building.



(e) (f) (g) (h)

Figure 19: IDR diagram for plan-B, 5-storey buildings with 2% target IDR in X-direction

428

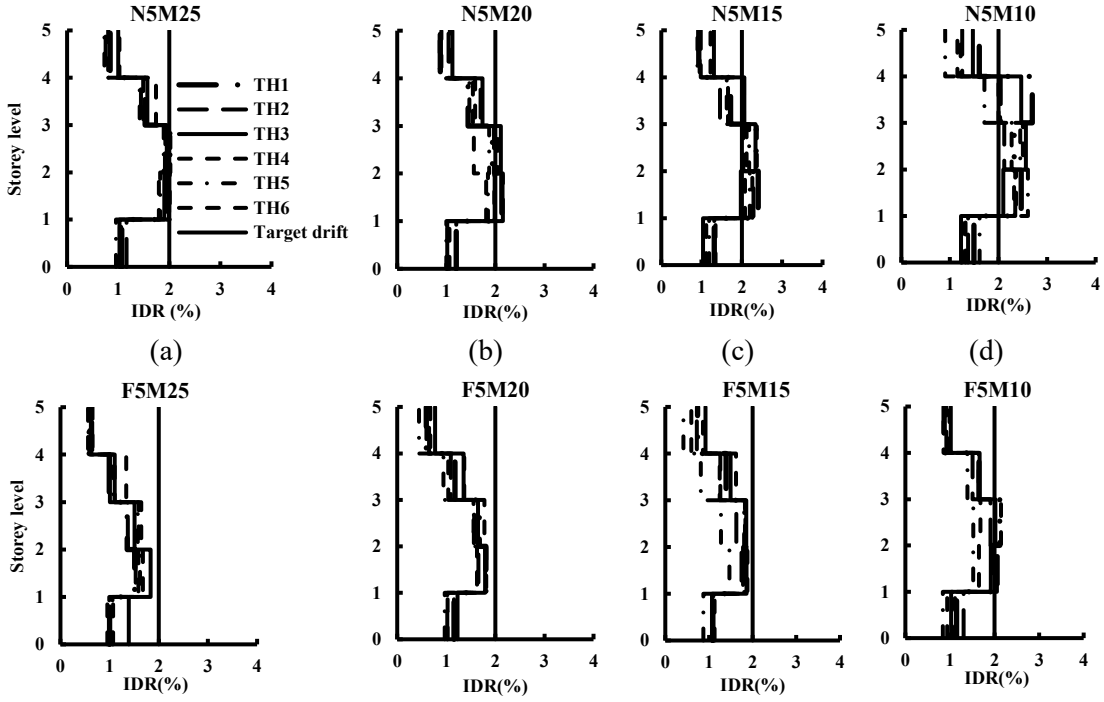
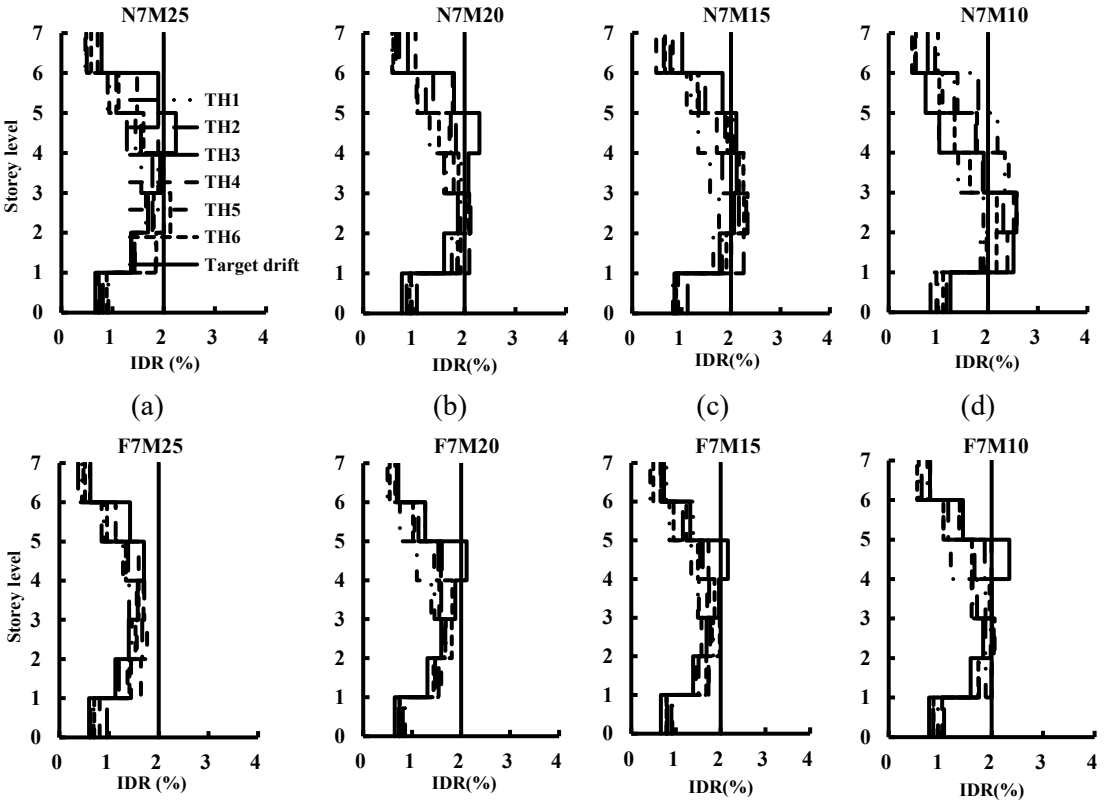


Figure 20: IDR diagram for plan-B, 5-storey buildings with 2% target IDR in Y-direction

429



(e) (f) (g) (h)

Figure 21: IDR diagram for plan-B, 7-storey buildings with 2% target IDR in X-direction

Figures (21)–(22) present the IDR profiles along the storey height for the CFRP-strengthened and unstrengthened 7-storey buildings in the two orthogonal directions (X and Y).

In the X-direction, the maximum IDR for the unstrengthened M10-grade concrete building is 2.6%, which decreases to 2.4% after CFRP strengthening. For the M15-grade building, the maximum IDR decreases from 2.4% in the unstrengthened condition to 2.2% in the CFRP-strengthened condition. Similarly, the maximum IDR decreases from 2.3% to 2.1% for the M20-grade building and from 2.3% to 1.8% for the M25-grade building.

In the Y-direction, the maximum IDR for the unstrengthened M10-grade concrete building is 2.5%, which decreases to 2.2% after CFRP strengthening. For the M15-grade building, the maximum IDR decreases from 2.3% in the unstrengthened condition to 2.1% in the CFRP-strengthened condition. For the M20-grade building, the maximum IDR decreases from 2.4% to 2.1%, while for the M25-grade building, it decreases from 2.2% to 1.7% following CFRP strengthening. Overall, the results demonstrate that CFRP strengthening reduces the maximum IDR response in both orthogonal directions, with the magnitude of reduction varying with the concrete grade.

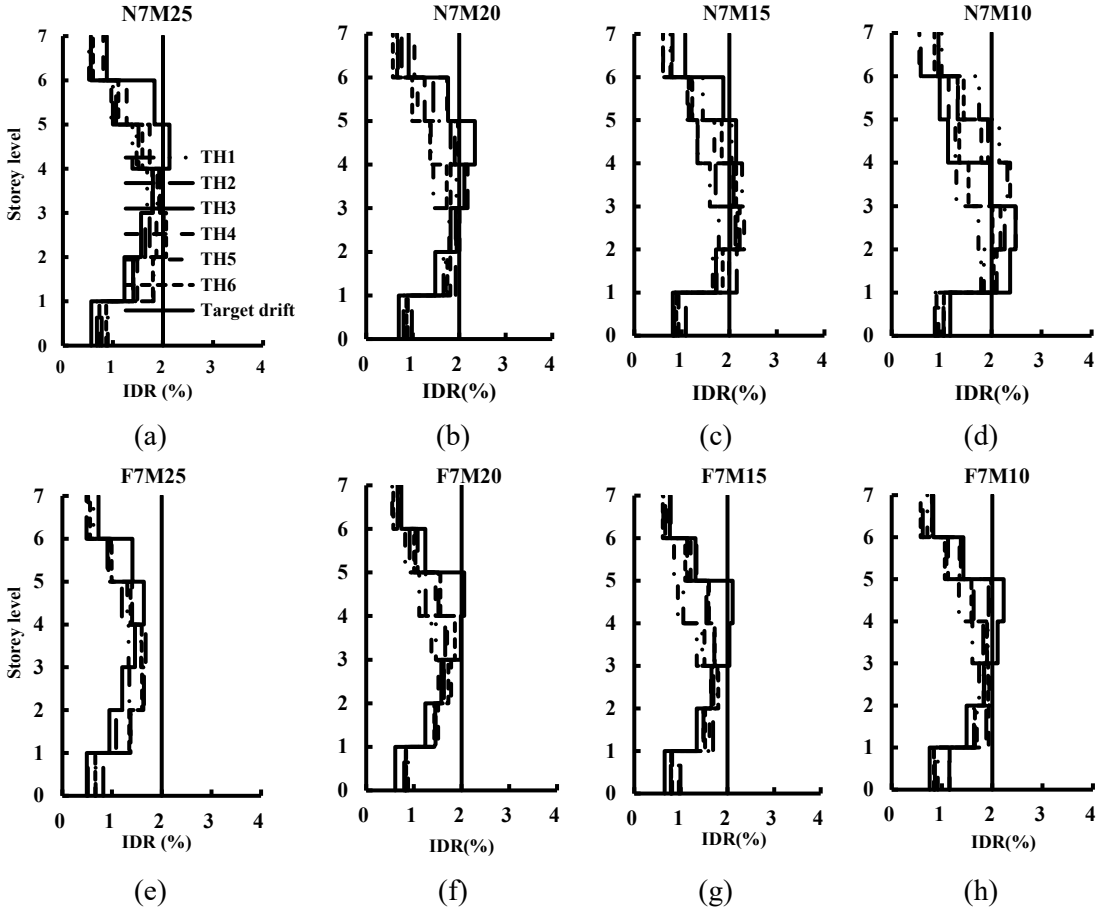


Figure 22: IDR diagram for plan-B, 7-storey buildings with 2% target IDR in Y-direction

446

447 Figures 23a and 23b illustrate the comparison of the average IDR ratios of strengthened to
448 those of the unstrengthened 5- and 7-storey plan B models, against varying concrete grades.
449 Comparing the achieved average IDR ratios with the predicted trend line (bold line) derived
450 for 5- and 7-storey building models using Equation (6), the variations are found to 4% and 3%
451 respectively. This indicates that Equation (6) can predict the probable the average IDR ratios
452 of strengthened to those of the unstrengthened with good accuracy.

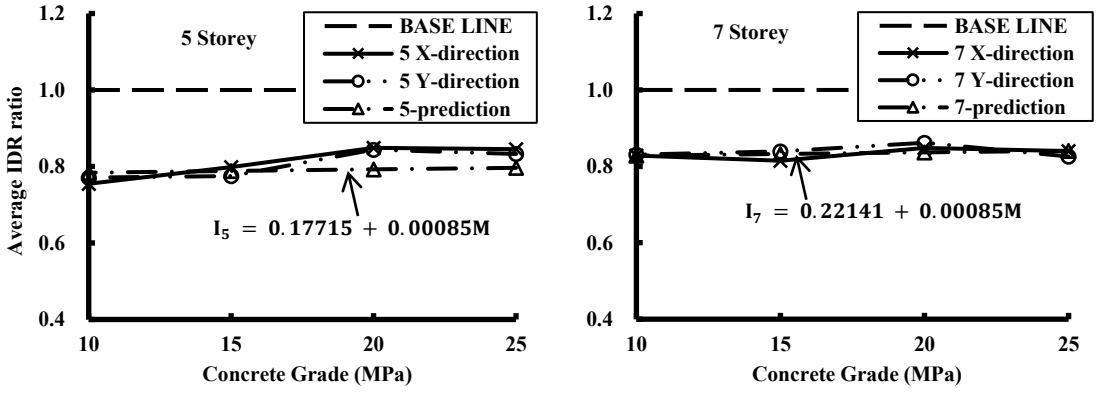
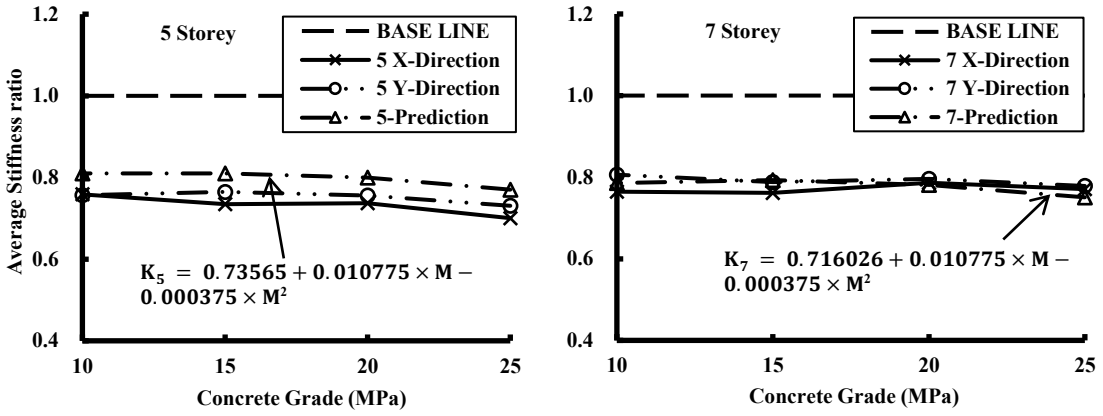


Figure 23: Average IDR ratio *Vs* Concrete Grade (MPa)

453

Figures 24(a) and 24(b) compare the average building stiffness ratios of the unstrengthened and CFRP-strengthened 5- and 7-storey Plan B building models for different concrete grades. The predicted trendlines (shown as bold lines), generated using Equation (11), are compared with the average building stiffness ratios obtained from NLTHA. The maximum deviations between the predicted and analytical building stiffness ratios are 8% and 4% for the 5- and 7-storey building models, respectively. These results demonstrate good agreement between the predicted and analytical building stiffness ratios, thereby confirming the applicability of the proposed predictive equation to building models with different plan configurations and heights.



(a) (b)

Figure 24: Average building Stiffness ratio *Vs* Concrete Grade (MPa)

6. Summary and Conclusions

The present investigation evaluates the effectiveness of externally bonded UHM-CFRP strengthening for improving the seismic performance of multi-storey reinforced concrete (RC) frame buildings with different levels of concrete strength deterioration. To this end, 4-, 6-, 8- and 10-storey RC buildings were designed using the Direct Displacement-Based Design (DDBD) methodology with a target inter-storey drift ratio (IDR) of 2%. The adopted numerical models are first validated against published experimental results. The M25, M20, M15, and M10 concrete grade buildings are investigated. Nonlinear time-history analyses were subsequently performed using spectrum-compatible ground motions, and the influence of UHM-CFRP strengthening was evaluated in terms of inter-storey drift ratio (IDR) and building lateral stiffness. Generalized predictive relationships were further developed to estimate the IDR ratio and building stiffness ratio as functions of concrete grade and building height. The proposed relationships were subsequently examined using independent building configurations to assess their applicability beyond the configurations used for model development.

The following broad conclusions can be drawn:

1. CFRP strengthening substantially improves the seismic response of RC frame buildings with reduced concrete strength. The results show consistent reductions in maximum and average IDR, bringing the response of lower-strength concrete buildings closer to that of the corresponding un-strengthened M25 buildings. Maximum IDR reductions of 31.5%, 26.6%, and 21.2% are observed for the M20, M15, and M10 4-storey buildings, respectively.
2. UHM-CFRP strengthening significantly enhances the lateral stiffness of the buildings. The increase in stiffness is observed for all investigated concrete grades and building heights, with the magnitude of improvement varying with both concrete grade and number of storeys. For example, the maximum stiffness increases for the M10 buildings are 40.52%, 17.38%, 45.77%, and 42.29% for the 4-, 6-, 8- and 10-storey buildings, respectively.
3. The effectiveness of CFRP strengthening is influenced by both the extent of concrete-strength deterioration and building height. The strengthening considerably mitigates the adverse effects of reduced concrete strength, with the response of CFRP-strengthened M10 buildings becoming comparable to that of the corresponding un-strengthened M25 buildings.
4. Generalized predictive equations are developed for estimating the IDR ratio and building stiffness ratio. These relationships incorporate concrete grade and building height, thereby providing a simple and computationally efficient approach for the preliminary estimation of the seismic response of CFRP-strengthened RC buildings without performing a complete nonlinear time-history analysis for every case.
5. The proposed predictive relationships show good agreement with independent numerical results. For the 5- and 7-storey buildings with different plan configurations, deviations in predicted IDR ratios are approximately 4% and 3%, while those in stiffness ratios are 8% and 4%, respectively.

In summary, the study demonstrates that externally bonded UHM-CFRP strengthening can effectively mitigate the adverse seismic effects associated with concrete-strength deterioration by reducing inter-storey drift and enhancing lateral stiffness. The proposed predictive relationships provide a practical tool for preliminary seismic assessment and retrofit decision-making for CFRP-strengthened RC frame buildings.

Author Contributions:

TAS – Conceptualization; Investigation; Numerical modelling; Formal analysis; Validation; Writing – original draft. **MSS** – Conceptualization; Methodology; Interpretation; Writing – review and editing; Final approval.

Funding:

No funds, grants, or other support was received.

Data availability:

Data will be made available on reasonable request.

Acknowledgement:

The authors sincerely thank their supervisors for their expert guidance, critical review, and continuous support throughout this research. The authors also acknowledge the Pacific Earthquake Engineering Research (PEER) Ground Motion Database for providing the earthquake ground motion records used in this study and the contributors of the published experimental studies used for model validation.

Declarations

Conflict of interest: The authors have no conflicts of interest to declare that are relevant to the content of this article.

Ethics approval: Relevant ethical requirements are compiled.

Consent: All authors have contributed to the article, read and approved the final version of the paper for submission to *Bulletin of Earthquake Engineering*.

Reference

ACI 440.2R-17, Guide for the Design and Construction of Externally Bonded FRP Systems for Strengthening Concrete Structures.

Akram Jawdhari, A.M.ASCE'; Abheetha Peiris, M.ASCE[2], Amir Fam, F.ASCE[3]; and Issam Harik, MLASCE. "Evaluation of Spliced UHM CFRP Strip Panels for Strengthening Steel Beams. "C 2022 American Society of Civil Engineers DOI: 1961/(ASCE)CC 1943-5614.0001275.

Alaa O. Swesi , Demitrios M. Cotsovos, Dimitri V. Val 2022,"Effect of CFRP strengthening on response of RC columns to lateral static and impact loads" Composite Structures Volume 287. https://doi.org/10.1016/j.compstruct.2022.115356

Antonopoulos, C.P., Triantafillou, T.C., 2003. Experimental investigation of FRP-strengthened RC beam-column joints. Journal of Composites for Construction 7(1), 39–49.

Bakis, C.E., Bank, L.C., Brown, V.L., Cosenza, E., Davalos, J.F., Lesko, J.J., Machida, A., Rizkalla, S.H., Triantafillou, T.C., 2002. Fiber-reinforced polymer composites for construction—State-of-the-art review. Journal of Composites for Construction 6(2), 73–87.

Balsamo, A., Colombo, A., Manfredi, G., Negro, P., Prota, A., 2005. Seismic behavior of a full-scale RC frame repaired using CFRP laminates. Engineering Structures 27, 769–780.

Binici, B., Mosalam, K.M., 2007. Analysis of reinforced concrete columns retrofitted with fiber reinforced polymer lamina. Composites Part B: Engineering 38, 265–276.

Bousias, S., Spathis, A.-L., Fardis, M.N., 2007. Seismic retrofitting of columns with lap spliced smooth bars through FRP or concrete jackets. Journal of Earthquake Engineering 11(5), 653–674.

Bureau of Indian Standards, *IS 1893 (Part 1): 2016: Criteria for Earthquake Resistant Design of Structures—Part 1: General Provisions and Buildings*, New Delhi, India, 2016.

Colomb, F., Tobbi, H., Ferrier, E., Hamelin, P., 2008. Seismic retrofit of reinforced concrete short columns by CFRP materials. Composite Structures 82(4), 475–487.

559 Del Vecchio, C., Di Ludovico, M., Prota, A., 2021. Cost and Effectiveness of Fiber-
560 Reinforced Polymer Solutions for the Large-Scale Mitigation of Seismic Risk in Reinforced
561 Concrete Buildings. Polymers 13(17), 2962. https://doi.org/10.3390/polym13172962

562 Del Zoppo, M., Di Ludovico, M., Balsamo, A., Prota, A., Manfredi, G., 2017. FRP for shear-
563 controlled RC columns: experience from earthquakes and experimental analysis. Composites
564 Part B: Engineering 129, 47–97. https://doi.org/10.1016/j.compositesb.2017.07.028

565 Di Ludovico, M., Manfredi, G., Mola, E., Negro, P., Prota, A., 2008. Seismic behavior of a
566 full-scale RC structure retrofitted using GFRP laminates. Journal of Structural Engineering
567 (ASCE) 134(5), 810–821.

568 Eid, R., Paultre, P., 2017. Compressive behavior of FRP-confined reinforced concrete
569 columns. Engineering Structures 132, 518–530.
570 https://doi.org/10.1016/j.engstruct.2016.11.052

571 Engindeniz, M., L. F. Kahn, and A.-H. Zureick. 2005. "Repair and strengthening of
572 reinforced concrete beam-column joints: State of the art." ACT Struct. J. 102 (2): 187-197,
573 https://doi.org/10.14359/14269.

574 Eslami, A., Ronagh, H.R., 2013. Effect of FRP wrapping in seismic performance of RC
575 buildings with and without special detailing—a case study. Composites Part B: Engineering
576 45(1), 1265–1274. Journal of Earthquake Engineering 28(7), 1914–1932.
577 https://doi.org/10.1080/13632469.2023.2256891

578 European Committee for Standardization (CEN), *EN 1998-1:2004+A1:2013 — Eurocode 8:*
579 *Design of Structures for Earthquake Resistance – Part 1: General Rules, Seismic Actions and*
580 *Rules for Buildings*, Brussels, Belgium, 2013.

581 Ghobarah, A., El-Attar, M., Aly, N.M., 2000. Evaluation of retrofit strategies for reinforced
582 concrete columns: a case study. Engineering Structures 22(5), 490–501.

583 Hadigheh, S.A., Mahini, S.S., Maheri, M.R., 2014. Seismic Behavior of FRP-Retrofitted
584 Reinforced Concrete Frames. Journal of Earthquake Engineering 18(8), 1171–1197.
585 https://doi.org/10.1080/13632469.2014.926301

586 Işık, E., Shao, Y.-B., Hadzima-Nyarko, M., Radu, D., Bulajic, B., Lozancic, S., 2026.
587 Enhancing the seismic safety of upgraded RC buildings using FRP retrofitting: analytical and

588 field evidence from the 2023 Kahramanmaraş earthquakes. Bulletin of Earthquake
589 Engineering 24, 1467–1501. https://doi.org/10.1007/s10518-025-02338-z

590 Jafari, S., Mahini, S.S., 2023. Enhancement of the Fragility Capacity of RC Frames Using
591 FRPs with Different Configurations at Joints. Polymers 15(3), 618.
592 https://doi.org/10.3390/polym15030618

593 Ji, G., G. Li, and W. Alaywan. 2013. "A new fire resistant FRP for externally bonded
594 concrete repair." Constr. Build. Mater. 42: 87-96. https:ال
595 doi.org/10.1016/j.conbuildmat.2013.01.008.

596 Karayannis, C.G., Sirkelis, G.M., 2008. Strengthening and rehabilitation of RC beam-column
597 joints using carbon-FRP jacketing and epoxy resin injection. Earthquake Engineering &
598 Structural Dynamics 37, 769–790.

599 Kumar, in Software for Generation of Spectrum Compatible Time History. 13th World
600 Conference on Earthquake Engineering, August1-6, Canada, Paper No. 2096, 2004.

601 Lam, L., Teng, J.G., 2003. Design-oriented stress–strain model for FRP-confined concrete.
602 Construction and Building Materials 17, 471–489

603 Li, L., Guo, Y., Liu, F., Bungey, J., 2006. An experimental and numerical study of the effect
604 of thickness and length of CFRP on performance of repaired reinforced concrete beams.
605 Construction and Building Materials 20, 901–909..

606 Mazza, F., Mazza, M., 2019. Seismic retrofitting of gravity-loads designed r.c. framed
607 buildings combining CFRP and hysteretic damped braces. Bulletin of Earthquake
608 Engineering 17, 3423–3445. https://doi.org/10.1007/s10518-019-00593-5

609 Mosallam, A.S., Banerjee, S., 2007. Shear enhancement of reinforced concrete beams
610 strengthened with FRP composite laminates. Composites Part B: Engineering 38, 781–793.

611 M.R. Esfahania , M.R. Kianoushb, A.R. Tajari 2007.“ Flexural behaviour of reinforced
612 concrete beams strengthened by CFRP sheets” Engineering Structures Volume 29, Issue 10,.
613 https://doi.org/10.1016/j.engstruct.2006.12.008.

614 Niroomandi, A., Maheri, A., Maheri, M.R., Mahini, S.S., 2010. Seismic performance of
615 ordinary RC frames retrofitted at joints by FRP sheets. Engineering Structures 32(8), 2326–
616 2336

Ozcan, O., Binici, B., Ozcebe, G., 2008. Improving seismic performance of deficient reinforced concrete columns using carbon fiber-reinforced polymers. Engineering Structures 30, 1632–1646.

Pacific Earthquake Engineering Research Center (PEER). 2026. "PEER NGA-West2 Ground Motion Database." University of California, Berkeley. PEER NGA-West2 Ground Motion Database

Pampanin, S., Bolognini, D., Pavese, A., 2007. Performance-based seismic retrofit strategy for existing RC frame systems using FRP composites. Journal of Composites for Construction (ASCE) 11(2), 211–226.

Pohoryles, D.A., Minas, S., Melo, J., Bournas, D.A., Varum, H., Rossetto, T., 2024. A Novel FRP Retrofit Solution for Improved Local and Global Seismic Performance of RC Buildings: Development of Fragility Curves and Comparative Cost-Benefit Analyses.

Priestley MJN, Calvi GM, Kowalsky MJ. Displacement-Based Seismic Design of Structures. IUSS Press: Pavia, 2007.

Promis, G., Ferrier, E., Hamelin, P., 2009. Effect of external FRP retrofitting on reinforced concrete short columns for seismic strengthening. Composite Structures 88, 367–379.

Prota, A., Nanni, A., Manfredi, G., Cosenza, E., 2004. Selective upgrade of underdesigned reinforced concrete beam-column joints using carbon fiber-reinforced polymers. ACI Structural Journal 101(5), 699–707.

Rabinovitch, O., Frostig, O., 2003. Experiments and analytical comparison of RC beams strengthened with FRP composites. Composites Part B: Engineering 34, 663–677.

SAP2000 v 21.2.0 Nonlinear Educational Version (Computer and Structures luc, Berkley, 2000).

S. Choudhury and S. M. Singh.2013. "A Unified Approach to Performance-Based Design of RC Frame Buildings. " J. Inst. Eng. India Ser. A (May-July 2013) 94(2):73-82 DOI 10.1007/s40030-013-0037-8.

Seible, F., Priestley, M.J.N., Hegemier, G.A., Innamorato, D., 1997. Seismic retrofit of RC columns with continuous carbon fiber jackets. Journal of Composites for Construction (ASCE) 1(2), 52–62.

646 Shaat, A., and A. Fam. 2007. "Finite element analysis of slender HSS columns strengthened
647 with high modulus composites." Steel Compos. Struct. 7 (1): 19-34.
648 https://doi.org/10.12989/scs.2007.7.1.019.

649 Sheikh, S., Li, Y., 2007. Design of FRP confinement for square concrete columns.
650 Engineering Structures 29(6), 1074–1083. https://doi.org/10.1016/j.engstruct.2006.07.016

651 Thermou, G. E., and A. S. Elnashai. 2006. "Seismic retrofit schemes for RC structures and
652 local–global consequences." Prog. Struct. Engng Mater. 8: 1-15.
653 https://doi.org/10.1002/pse.208

654 Teng, J.G., Lam, L., 2002. Compressive behaviour of carbon fiber reinforced polymer-
655 confined concrete in elliptical columns. Journal of Structural Engineering (ASCE) 128(12),
656 1535–1543.

657 Thermou, G. E., Bousselham, A. 2010. "State of research on seismic retrofit of RC beam-
658 column joints with externally bonded FRP." J. Compos. Constr. 14 (1): 49-61.
659 https://doi.org/10.1061/(ASCE)CC.1943-5614.0000049

660 Wu, C., X. L. Zhao, W. K. Chiu, R. Al-Mahaidi, and W. H. Duan. 2013. "Effect of fatigue
661 loading on the bond behaviour between UHM CFRP plates and steel plates." Composites,
662 Part B 50: 344-353 doi.org/10.1016/j.compositesb.2013.02.040.

663 Zou, X.K., Teng, J.G., De Lorenzis, L., Xia, S.H., 2007. Optimal performance-based design
664 of FRP jackets for seismic retrofit of reinforced concrete frames. Composites Part B:
665 Engineering 38, 584–597. https://doi.org/10.1016/j.compositesb.2006.07.016

666 Zhu, F., Zhang, M., Zhang, D., Wang, D., Wang, Z., Zhang, Y., 2025. Seismic behavior of
667 FRP-retrofitted rectangular RC columns subjected to oblique horizontal earthquake actions.
668 Construction and Building Materials 482, 141737.
669 https://doi.org/10.1016/j.conbuildmat.2025.141737